J|A|C|S
ARTICLES
Published on Web 02/10/2004

Density Functional Theory Calculations and Exploration of a Possible Mechanism of N_2 Reduction by Nitrogenase

Uwe Huniar,[†] Reinhart Ahlrichs,*[,†] and Dimitri Coucouvanis*[,‡]

Contribution from the Department of Chemistry, University of Karlsruhe, Karlsruhe, Germany, and Department of Chemistry, The University of Michigan, Ann Arbor, Michigan 48109-1055

Received September 18, 2003; Revised Manuscript Received December 9, 2003; E-mail: reinhart.ahlrichs@chemie.uni-karlsruhe.de; dcouc@umich.edu

Abstract: Density functional theory (DFT) calculations have been performed on the nitrogenase cofactor, FeMoco. Issues that have been addressed concern the nature of M−M interactions and the identity and origin of the central light atom, revealed in a recent crystallographic study of the FeMo protein of nitrogenase (Einsle, O.; et al. *Science* **2002**, *297*, 871). Introduction of Se in place of the S atoms in the cofactor and energy minimization results in an optimized structure very similar to that in the native enzyme. The nearly identical, short, lengths of the Fe−Fe distances in the Se and S analogues are interpreted in terms of M−M weak bonding interactions. DFT calculations with O or N as the central atoms in the FeMoco marginally support the assignment of the central atom as N rather than O. The assumption was made that the central atom is the N atom, and steps of a catalytic cycle were calculated starting with either of two possible states for the cofactor and maintaining the same charge throughout (by addition of equal numbers of H^+ and e^-) between steps. The states were $[(Cl)Fe^{II}_6Fe^{III}Mo^{IV}S_9(H^+)_3N^{3-}(Gl)(Im)]^{2-}$, [**I-N-3H**]$^{2-}$, and $[(Cl)Fe^{II}_4Fe^{III}_3Mo^{IV}S_9(H^+)_3N^{3-}(Gl)(Im)]$, [**I-N-3H**]^{0} (Gl = deprotonated glycol; Im = imidazole). These are the triply protonated ENDOR/ESEEM [**I-N**]$^{5-}$ and Mössbauer [**I-N**]$^{3-}$ models, respectively. The proposed mechanism explores the possibilities that (a) redox-induced distortions facilitate insertion of N_2 and derivative substrates into the Fe_6 central unit of the cofactor, (b) the central atom in the cofactor is an exchangeable nitrogen, and (c) the individual steps are related by H^+/e^- additions (and reduction of substrate) or aquation/dehydration (and distortion of the Fe_6 center). The ΔE's associated with the individual steps of the proposed mechanism are small and either positive or negative. The largest positive ΔE is +121 kJ/mol. The largest negative ΔE of −333 kJ/mol is for the FeMoco with a N^{3-} in the center (the isolated form) and an intermediate in the proposed mechanism.

Introduction

Single-crystal X-ray structure determinations of the MoFe protein component of nitrogenases from various sources[1−3] have revealed the structure of the common octanuclear $MoFe_7S_9$ catalytic center to various levels of resolution. This center consists (Figure 1) of two cuboidal subunits, $MoFe_3S_3$ and Fe_4S_3, bridged by three μ_2-S^{2-} ligands and shows the six central Fe atoms arranged in a trigonal prismatic Fe_6 unit. The coordinatively unsaturated, three-coordinate Fe atoms, within the Fe_6 prism, were unusual features that received particular attention in studies concerned with the structure and function of the nitrogenase cofactor.

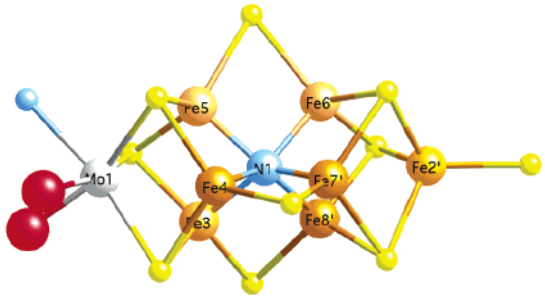

Figure 1. Idealized structure of the nitrogenase cofactor. [4] Only the donor atoms of the terminal ligands (S, cys; N, His; and 2O, homocitrate) are shown. The above numbering scheme follows the one used in the MoFe structure determinations[1−4] and is retained in all other figures and tables.

The most recent structure determination[4] of the *A. vinelandii* MoFe protein at 1.16 Å resolution revealed a previously undetected light atom in the center of the FeMoS center encapsulated by the six Fe atoms of the central Fe_6 unit (Figure 1). This new finding altered the coordination geometry for each of the six central Fe atoms to four-coordinate, trigonal pyra-

[†] University of Karlsruhe.
[‡] The University of Michigan.

(1) (a) Kim, J.; Rees, D. C. *Nature* **1992**, *360*, 553. (b) Kim, J.; Rees, D. C. *Science* **1992**, *257*, 1677. (c) Chan, M. K.; Kim, J.; Rees, D. C. *Science* **1993**, *260*, 792. (d) Georgiadis, M. M.; Komiya, H.; Woo, D.; Kornuc, J. J.; Rees, D. C. *Science* **1992**, *257*, 1653. (e) Kim, J.; Woo, D.; Rees, D. C. *Biochemistry* **1993**, *32*, 7104. (f) Schindelin, N.; Kisker, C.; Schlessman, J. L.; Howard, J. B.; Rees, D. C. *Nature* **1997**, *387*, 370. (g) Strop, P.; Takahara, P. M.; Chiu, H.-J.; Angove, H. C.; Burgess, B. K.; Rees, D. C. *Biochemistry* **2001**, *40*, 651.
(2) Bolin, J. T.; Ronco, A. E.; Morgan, T. V.; Mortenson, L. E.; Xuong, N. *Proc. Natl. Acad. Sci. U.S.A.* **1993**, *90*, 1078.
(3) Mayer, S. M.; Lawson, D. M.; Gormal, C. A.; Roe, S. M.; Smith, B. E. *J. Mol. Biol.* **1999**, *292*, 871.
(4) Einsle, O.; Teczan, F. A.; Andrade, S. L. A.; Schmid, B.; Yoshida, M.; Howard, J. B.; Rees, D. C. *Science* **2002**, *297*, 1696.

10.1021/ja030541z CCC: $27.50

midal, refocused the interest in structural features of the cofactor, and introduced new questions regarding the nature and origin of the light atom. The latter initially[4] was proposed to be a N atom. This proposal is supported by a number of recent density functional theory (DFT) calculations which indicate[5−7] the light atom to be N rather than O or C.

Prior to the discovery of the central light atom in the 6Fe cavity, two different descriptions for the nitrogenase cofactor in the $S = {}^3/_2$ ground state were proposed on the basis of spectroscopic data analyses. Data obtained by Mössbauer spectroscopy[8] have been interpreted in terms of the [(His)Mo^{IV}-$Fe^{III}{}_3Fe^{II}{}_4(S^{2-})_9$(h-citr^{2-})(cys$^-$)] description, [**I**].

Data obtained by electron nuclear double resonance (ENDOR) and electron spin−echo envelope modulation (ESEEM) spectroscopy[9] have been analyzed in terms of the [(His)$Mo^{IV}Fe^{III}$-$Fe^{II}{}_6(S^{2-})_9$(h-citr^{2-})(cys$^-$)]$^{2-}$ description, [**I**]$^{2-}$.

The [**I**]$^{2-}$ model was found preferable to [**I**] on the basis of an early DFT study[10] of the electronic structure of the nitrogenase cofactor, in the absence of the central light atom. Upon introduction of a N^{3-} central atom, the original electronic descriptions [**I**] and [**I**]$^{2-}$ are now designated as [(His)Mo^{IV}-$Fe^{III}{}_3Fe^{II}{}_4(S^{2-})_9(N^{3-})$(h-citr^{2-})(cys$^-$)]$^{3-}$, [**I-N**]$^{3-}$, and [(His)$Mo^{IV}$-$Fe^{III}Fe^{II}{}_6(S^{2-})_9(N^{3-})$(h-citr^{2-}) (cys$^-$)],$^{5-}$ [**I-N**]$^{5-}$, respectively.

In the most recent DFT study, the electronic description of the resting cofactor was reevaluated,[7] and with the central light atom included as N^{3-}, the "Mössbauer model", [**I-N**]$^{3-}$, was found to be a better choice than [**I-N**].$^{5-}$ In this study, the calculated Mössbauer spectra and redox potential for [**I-N**]$^{3-}$ were found to be in better agreement with experimental results. In the same study, a doubly protonated form of [**I-N**]$^{5-}$ was also suggested as a possible alternate model. DFT calculations by Dance[6] and by Hinneman and Nørskov,[5] based on the [**I-N**]$^{3-}$ description, concluded that the interactions of dinitrogen with the FeMo-cofactor occur on the surface of the Fe_6 prism.

The rather short M−M distances in the FeMo-cofactor, Fe−Fe 2.60(1), 2.66(1) Å, Fe−Mo 2.69(1) Å, and the small number of total valence electrons available for bonding are features quite similar to structural and electronic characteristics of a series of synthetic clusters we have reported recently.[11,12] These clusters contain the cuboidal $MoFe_3S_3$ core as a common structural unit and, on the basis of DFT calculations, have been shown to display[13] weak M−M bonding interactions.

Recently, we have undertaken DFT studies of the nitrogenase cofactor to explore the origin and determine the nature of the central light atom and its importance as a structure stabilizing feature. In this paper, we report the results of these studies, and we examine a possible mechanism of nitrogenase function. This mechanism is based on pronounced structural changes that accompany oxidation−reduction of the M_8S_9N core and describes the introduction of N, in the center of the cofactor, as part of the mechanism of the nitrogen fixation reaction. Most of the calculated cofactor-intermediate structures in the stepwise reduction of N_2 (Figure 3, Chart 1) are very similar to intermediates reported for the reduction of dinitrogen using Mo−phosphine complexes by Chatt and co-workers.[14] They are also similar to structurally characterized intermediates involved in the recently reported catalytic reduction of dinitrogen to ammonia[15] by the sterically hindered mononuclear ($HIPTN_3$)-MoN_2 complex ($HIPTN_3$ = the hexaisopropyl terphenyl derivative of triethylene tetramine).

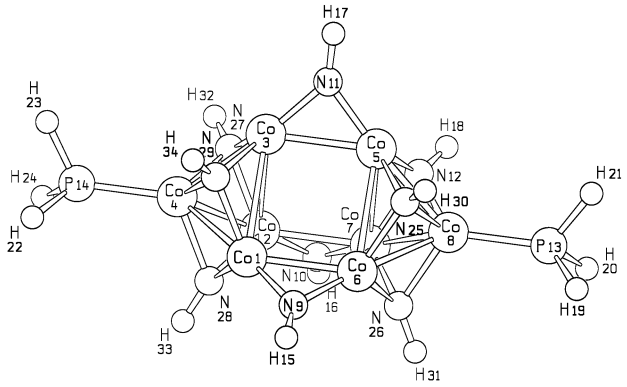

Figure 2. Optimized structure of the hypothetical $[Co_8(\mu_3\text{-NH})_6((\mu_2\text{-NH})_3(PH_3)_2]^-$ cluster.[32]

In the past, a multitude of theoretical papers[5−7,10,16−24] have dealt with the electronic structure of the cofactor and mechanisms of substrate binding and activation. These papers have laid the foundations upon which this work is based.

Methods

All calculations have been performed with the program package Turbomole[25] using density functional theory (DFT). The BP86[26] and partly B3-LYP [27] functionals have been used together with the SV(P)[28] (split valence plus polarization, except for H) and TZVP[29] (triple-ζ valence plus polarization), respectively, basis sets. No spin restrictions

(5) Hinneman, B.; Nørskov, J. K. *J. Am. Chem. Soc.* **2003**, *125*, 1466.
(6) Dance, I. *Chem. Commun*. **2003**, 324−325.
(7) Lovell, T.; Liu, T.; Case, D. A.; Noodleman, L. *J. Am. Chem. Soc.* **2003**, *125*, 8377−8383.
(8) Yoo, S. J.; Angove, H. C.; Papaefthymiou, V.; Burgess, B. K.; Munck, E.. *J. Am. Chem. Soc.* **2000**, *122*, 4926.
(9) (a) Lee, H.-I.; Hales, B. J.; Hoffman, B. M. *J. Am. Chem. Soc.* **1997**, *119*, 11395. (b) True, A. E.; Nelson, M. J.; Venters, R. A.; Orme-Johnson, W. H.; Hoffman, B. M. *J. Am. Chem. Soc.* **1988**, *110*, 1935.
(10) Lovell, T.; Li, J.; Liu, T.; Case, D. A.; Noodleman, L. *J. Am. Chem. Soc.* **2001**, *123*, 12392.
(11) Han, J.; Beck, K.; Ockwig, N.; Coucouvanis, D. *J. Am. Chem. Soc.* **1999**, *121*, 10448.
(12) Coucouvanis, D.; Han, J.; Moon, N. *J. Am. Chem. Soc.* **2002**, *124*, 216.
(13) Nava, P.; Han, J.; Ahlrichs, R.; Coucouvanis, D., submitted for publication.
(14) (a) Chatt, J.; Dilworth, J. R.; Richards, R. L. *Chem. Rev.* **1978**, *78*, 589. (b) Pickett, C. J. *J. Biol. Inorg. Chem*. **1996**, *1*, 601−606.
(15) Schrock, R.; Yandulov, D. *Science* **2003**, *301*, 76.
(16) (a) Lovell, T.; Li, J.; Case, D. A.; Noodleman, L. *J. Am. Chem. Soc*. **2002**, *124*, 4546. (b) Lovell, T.; Torres, R. A.; Han, W.-G.; Liu, T.; Case, D. A.; Noodleman, L. *Inorg. Chem*. **2002**, *41*, 5744. (c) Lovell, T.; Li, J.; Case, D. A.; Noodleman, L. *J. Biol. Inorg. Chem*. **2002**, *7*, 735.
(17) Deng, H.; Hoffmann, R. *Angew. Chem., Int. Ed. Engl.* **1993**, *32*, 1062.
(18) (a) Stavrev, K. K.; Zerner, M. C. *Chem.-Eur. J.* **1996**, *2*, 83. (b) Stavrev, K. K.; Zerner, M. C. *Theor. Chim. Acta* **1997**, *96*, 141. (c) Stavrev, K. K.; Zerner, M. C. *Int. J. Quantum Chem.* **1998**, *70*, 1159.
(19) (a) Dance, I. *Aust. J. Chem*. **1994**, *47*, 979. (b) Dance, I. *Chem. Commun*. **1997**, 165. (c) Dance, I. *Chem. Commun*. **1998**, 523. (d) Dance, I. *J. Biol. Inorg. Chem*. **1996**, *1*, 581.
(20) Siegbahn, P. E. M.; Westerberg, J.; Svensson, M.; Crabtree, R. H. *J. Phys. Chem. B* **1998**, *102*, 1615.
(21) Szilagyi, R. K.; Musaev, D. K.; Morokuma, K. *Inorg. Chem*. **2001**, *40*, 766.
(22) (a) Rod, T. H.; Hammer, B.; Nørskov, J. K. *Phys. Rev. Lett*. **1999**, *82*, 4054. (b) Rod, T. H.; Logadottir, A.; Nørskov, J. K. *J. Chem. Phys*. **2000**, *112*, 5343. (c) Rod, T. H.; Nørskov, J. K. *J. Am. Chem. Soc*. **2000**, *122*, 12751.
(23) (a) Durrant, M. C. *Inorg. Chem. Commun*. **2001**, *4*, 60. (b) Durrant, M. C. *Biochem. J*. **2001**, *355*, 569. (c) Durrant, M. C. *Biochemistry* **2002**, *41*, 13946. (d) Durrant, M. C. *Biochemistry* **2002**, *41*, 13934. (e) Gronberg, K.; Gormal, C.; Durrant, M.; Smith, B.; Henderson, R. *J. Am. Chem. Soc*. **1998**, *120*, 10613.
(24) (a) Barriere, F.; Pickett, C. J.; Talarmin, J. *Polyhedron* **2001**, *20*, 27. (b) Pickett, C. J. *J. Biol. Inorg. Chem*. **1996**, *1*, 601.
(25) Ahlrichs, R.; Bär, M.; Häser, M.; Horn, H.; Kölmel, C. *Chem. Phys. Lett.* **1989**, *162*, 165.
(26) (a) Perdew, J. P. *Phys. Rev. B* **1986**, *33*, 8822. (b) Perdew, J. P. *Phys. Rev. B* **1986**, *34*, 7046. (c) Becke, A. D. *Phys. Rev. A* **1988**, *38*, 3098.
(27) (a) Becke, A. D. *J. Chem. Phys*. **1993**, *98*, 5648. (b) Stevens, P. J.; Devlin, F. J.; Chablowski, C. F.; Frisch, M. J. *J. Phys. Chem*. **1994**, *98*, 11623.

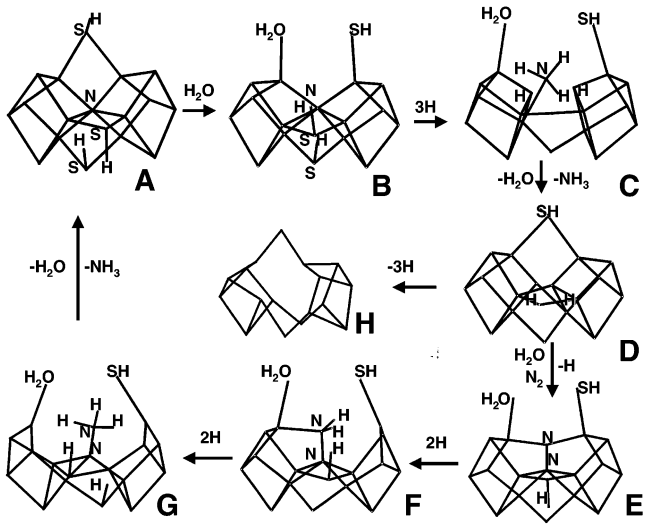

Figure 3. A mechanism for the catalytic reduction of N_2 by the FeMo-cofactor of nitrogenase.

Chart 1

Abbreviations used[a] for:	In Text	In Fig.3
$[(Cys)Fe^{II}_4Fe^{III}_3Mo^{IV}S_9(h\text{-}citr)(His)]$	**[I]**	
$[(Cl)Fe^{II}_6Fe^{III}Mo^{IV}S_9(Gl)(Im)]^{2-}$	$[\mathbf{I}]^{2-}$	**H**
$[(Cl)Fe^{II}_4Fe^{III}_3Mo^{IV}S_9(N)(Gl)(Im)]^{3-}$	$[\mathbf{I\text{-}N}]^{3-}$	
$[(Cl)Fe^{II}_6Fe^{III}Mo^{IV}S_9(N)(Gl)(Im)]^{5-}$	$[\mathbf{I\text{-}N}]^{5-}$	
$[(Cl)Fe^{II}_4Fe^{III}_3Mo^{IV}S_9(N)(H^+)_3(Gl)(Im)]$	**[I-N-3H]**	
$[(Cl)Fe^{II}_6Fe^{III}Mo^{IV}S_9(N)(H^+)_3(Gl)(Im)]^{2-}$	$[\mathbf{I\text{-}N\text{-}3H}]^{2-}$	**A**
$[(Cl)Fe^{II}_6Fe^{III}Mo^{IV}S_9(N)(H_2O)(H^+)_3(Gl)(Im)]^{2-}$		**B**
$[(Cl)Fe^{II}_6Fe^{III}Mo^{IV}S_9(NH_3)(H)_3(H_2O)(Gl)(Im)]^{2-}$		**C**
$[(Cl)Fe^{II}_6Fe^{III}Mo^{IV}S_9(H)_3(Gl)(Im)]^{2-}$		**D**
$[(Cl)Fe^{II}_6Fe^{III}Mo^{IV}S_9(N_2)(H^+)_2(H_2O)(Gl)(Im)]^{2-}$		**E**
$[(Cl)Fe^{II}_6Fe^{III}Mo^{IV}S_9(NNH_2)(H^+)_2(H_2O)(Gl)(Im)]^{2-}$		**F**
$[(Cl)Fe^{II}_6Fe^{III}Mo^{IV}S_9(NNH_3)(H^+)_3(H_2O)(Gl)(Im)]^{2-}$		**G**

have been made employing the pseudo Fermi smearing technique[30] together with a spin unrestricted Kohn−Sham formalism. All nuclear coordinates have been fully optimized. The RI-J[31]technique has been used together with the BP86 functional. Convergence criteria were set to 10^{-3} hartree/bohr in the norm of the gradients and 10^{-5} in energy change. Mulliken population analysis has been used to determine the charge and the spin density at all atoms. The effectiveness of the method used was tested on $[Co_8(\mu_3\text{-}NH)_6((\mu_2\text{-}NH)_3(PH_3)_2]^-$, a variant of the structurally characterized[32] $[Co_8(\mu_3\text{-}NPh)_6(\mu_2\text{-}NPh)_3(PPh_3)_2]^-$ cluster which is the only cluster known with a structure similar to that of the cofactor (Figure 2) but without a central light atom and μ-NPh ligands in place of the μ-S ligands. The results (Table 1) show that DFT using the B-P86 functional and SVP or TZVP basis sets describes the experimental structure sufficiently well.

The cofactor models and derivatives used in all calculations have the terminal cysteinyl ligand on the peripheral Fe atom replaced by Cl^-. The bidentate, homocitrate ligand bound to the Mo atom has been replaced by two oxygen donors and the carbon atoms attached to them making this ligand essentially a deprotonated ethylene glycol. Imidazole is used in place of the terminal Mo-bound histidine. A calculation using CH_3S^- instead of Cl^- as a terminal ligand on the peripheral Fe atom (Fe2′) also was carried out. The intramolecular distances and atomic charges in the CH_3S^- and Cl^- derivatives are not significantly different.

Table 1. Structure Data of $[Co_8(\mu_3\text{-}NH)_6(\mu_2\text{-}NH)_3\cdot(PH_3)_2]^-$, Calculated with the BP86 Functional

distances, Å	exp.	SVP	TZVP
Co1−Co6	2.439−2.479	2.395	2.428
Co1−Co2	2.721−2.773	2.706	2.759
Co1−Co4	2.386−2.413	2.342	2.368
Co−P	2.195−2.203	2.097	2.120

Table 2. Structures of the Energy Minimized $[\mathbf{I_E}]^{2-}$, $[\mathbf{I_E\text{-}X}]^{2-}$ Clusters (E = S and Se) and Comparison to the Structure of the Nitrogenase FeMo-Cofactor[4] [a]

	no X	X = N	X = O	X-ray[4]	no X, Se	X = N, Se
Mo−Fe5	2.75	2.77	2.77	2.67		
Mo−Fe3	2.67	2.78	2.77	2.69		
Mo−Fe4	3.05	2.77	2.79	2.73		
mean	*2.82(14)*	*2.77(1)*	*2.78(1)*	*2.70(2)*		
Fe5−Fe3	2.46	2.55	2.68	2.63	2.56	2.55
Fe3−Fe4	2.45	2.54	2.69	2.62	2.54	2.55
Fe5−Fe4	2.52	2.50	2.65	2.59	2.43	2.48
mean	*2.47(3)*	*2.53(2)*	*2.67(1)*	*2.61(1)*	*2.51(5)*	*2.53(3)*
Fe5−Fe6′	2.51	2.56	2.67	2.58	2.53	2.60
Fe3−Fe8′	2.41	2.54	2.64	2.58	2.50	2.58
Fe4−Fe7′	2.54	2.56	2.68	2.62	2.48	2.60
mean	*2.49(5)*	*2.55(1)*	*2.66(1)*	*2.59(2)*	*2.50(2)*	*2.59(1)*
Fe6′−Fe8′	2.46	2.62	2.75	2.65	2.57	2.62
Fe8′−Fe7′	2.53	2.63	2.74	2.67	2.57	2.63
Fe6′−Fe7′	2.55	2.56	2.68	2.64	2.58	2.56
mean	*2.51(3)*	*2.60(3)*	*2.72(3)*	*2.65(1)*	*2.57(1)*	*2.60(3)*
Fe6′−Fe2′	2.51	2.63	2.56	2.66		
Fe7′−Fe2′	2.59	2.70	2.63	2.67		
Fe8′−Fe2′	2.51	2.63	2.56	2.66		
mean	*2.54(3)*	*2.65(3)*	*2.58(3)*	*2.66(1)*		
Fe−X		2.00(6)	2.05(6)	2.00(2)		1.97(6)

[a] The numbering scheme follows that in Figure 1.

Results

M−M Interactions. Supporting evidence for M−M attractive interactions in the FeMoS clusters has been sought in calculations where the S^{2-} ligands are replaced by Se^{2-}. DFT calculations and energy minimization of the center-voided FeMoco, $[\mathbf{I}]^{2-}$ (with S^{2-} ligands), and also of the same cluster with Se^{2-} ligands in place of S^{2-} show virtually identical Fe−Fe distances in the $Mo^{IV}Fe^{III}Fe^{II}_6Se_9$ and $Mo^{IV}Fe^{III}Fe^{II}_6S_9$ cores (Table 2). Similar results have been obtained with the $[\mathbf{I\text{-}N}]^{2-}$ and $[\mathbf{I\text{-}N_{Se}}]^{2-}$ clusters (Table 2). In this case, however, the relative importance of Fe−Fe attractive interactions in stabilizing the structure is difficult to evaluate, and Fe−N bonding certainly plays an important role.

The Central Light Atom. Calculations aimed at identifying the nature of the central light atom **X** in the cofactor could start with the $[\mathbf{I\text{-}X}]^{n-}$ anion for either the ENDOR/ESEEM model[9] ($\mathbf{X} = O^{2-}$, $n = 4$ or $\mathbf{X} = N^{3-}$, $n = 5$) or the Mössbauer model[8] ($\mathbf{X} = O^{2-}$, $n = 2$ or $\mathbf{X} = N^{3-}$, $n = 3$).

We have minimized the energy and determined optimized structures for the cofactor, with O or N atoms (**X**) in the central Fe_6 unit and the formal description $[(Cl)Fe_7MoS_9X(Gl)(Im)]^{2-}$, $[\mathbf{I\text{-}X}]^{2-}$ (Table 2), and compared the results to the experimentally determined structure. In these calculations, the dianion rather

(28) Schäfer, A.; Horn, H.; Ahlrichs, R. *J. Chem. Phys.* **1992**, *97*, 2571.
(29) Schäfer, A.; Huber, C.; Ahlrichs, R. *J. Chem. Phys.* **1994**, *100*, 5829.
(30) Nava, P.; Sierka, M.; Ahlrichs, R. *Phys. Chem. Chem. Phys.* **2003**, *5*, 3372.
(31) Eichkorn, K.; Treutler, O.; Öhm, H.; Häser, M.; Ahlrichs, R. *Chem. Phys. Lett.* **1995**, *242*, 652.
(32) Link, H.; Fenske, D. *Z. Anorg. Allg. Chem.* **1999**, *625*, 1878−1884.

Table 3. Electronic Spin Vectors ($\alpha-\beta$) and Mulliken Population Analysis Charges for the Mechanistic Intermediates Shown in Figure 3 and Derived from [**I-N-3H**]$^{2-}$ (**A** → **G**) and the Two Electron Oxidized [**I-N-3H**] (**A^0** → **G^0**) Clusters[a]

atom	A	A^0	A-3H$^+$	A$_{SCH3}$	B	B^0	C	C^0	D	D^0	E	E^0	E$_{SCH3}$	F	F^0	G	G^0	H
Fe3, $\alpha-\beta$	+2.70	−2.62	−2.8	+2.82	−2.87	−3.07	−2.80	−1.81	+2.63	+2.67	−2.84	−3.01	−2.73	−2.98	−2.05	+3.06	−2.93	2.75
charge	**0.22**	**0.22**	**0.20**	**0.24**	**0.22**	**0.27**	**0.15**	**0.03**	**0.17**	**0.08**	**0.26**	**0.23**	**0.25**	**0.26**	**0.14**	**0.27**	**0.17**	**0.14**
Fe4, $\alpha-\beta$	−2.64	+2.79	−2.8	−2.08	−3.14	−2.63	−2.34	−2.73	2.20	+2.16	+2.71	+2.46	2.77	−2.60	−2.18	−2.87	+3.09	2.73
charge	**0.20**	**0.25**	**0.23**	**0.18**	**0.22**	**0.18**	**0.07**	**0.13**	**0.03**	**−0.01**	**0.24**	**0.28**	**0.25**	**0.24**	**0.19**	**0.17**	**0.27**	**0.14**
Fe5, $\alpha-\beta$	+2.83	+2.90	1.7	2.90	+3.17	−3.30	+3.05	+3.08	−2.96	−2.95	+2.73	+2.80	2.73	+3.15	+3.19	−2.72	−3.16	−2.49
charge	**0.21**	**0.23**	**0.17**	**0.22**	**0.27**	**0.33**	**0.17**	**0.24**	**0.11**	**0.12**	**0.24**	**0.28**	**0.23**	**0.24**	**0.29**	**0.13**	**0.24**	**0.05**
Fe6′, $\alpha-\beta$	−2.97	−2.91	1.7	−3.07	+3.17	+2.97	−3.00	−3.11	−3.14	−2.91	+2.72	2.69	2.55	+3.35	+3.34	+3.28	+2.88	−2.39
charge	**0.22**	**0.24**	**0.19**	**0.22**	**0.27**	**0.23**	**0.09**	**0.15**	**0.12**	**0.24**	**0.23**	**0.20**	**0.22**	**0.17**	**0.22**	**0.12**	**0.17**	**0.05**
Fe7′, $\alpha-\beta$	−1.17	−1.33	3.1	−2.47	−3.14	−2.62	2.91	−2.82	−2.94	−2.56	−3.12	−2.87	−3.12	+3.19	+2.38	−3.22	−3.03	−2.50
charge	**0.13**	**0.13**	**0.17**	**0.18**	**0.22**	**0.15**	**0.05**	**0.05**	**0.04**	**0.02**	**0.24**	**0.20**	**0.24**	**0.27**	**0.11**	**0.21**	**0.16**	**0.05**
Fe8′, $\alpha-\beta$	−2.88	−2.81	2.9	−2.98	+2.96	+2.65	−3.09	+2.41	+2.90	+2.69	+2.77	+2.67	2.72	−3.16	−2.72	+3.34	+3.12	−2.43
charge	**0.20**	**0.21**	**0.18**	**0.20**	**0.16**	**0.13**	**0.11**	**0.00**	**0.02**	**−0.07**	**0.20**	**0.20**	**0.20**	**0.22**	**0.15**	**0.24**	**0.24**	**0.04**
Fe2′, $\alpha-\beta$	+3.26	3.12	−2.5	3.21	−3.32	−3.08	3.24	2.78	+3.27	+3.23	−3.23	−2.98	−3.14	+3.33	+2.45	+3.35	+2.77	3.25
charge	**0.31**	0.27	**0.29**	**0.28**	**0.32**	**0.29**	**0.29**	**0.25**	**0.31**	**0.30**	**0.29**	**0.25**	**0.24**	**0.30**	**0.17**	**0.32**	**0.22**	**0.29**
Mo, $\alpha-\beta$	−0.19			−0.33	−0.89		+0.08		−0.22		−0.33		−0.33	0.27		0.37		−0.11
charge	**0.08**			0.08	**0.10**		**0.06**		**−0.02**		**0.06**		**0.06**	**0.07**		**0.003**		**0.008**
N1, $\alpha-\beta$	0.06						−0.02				−0.04		−0.03	0.03		**0.03**		
charge	**−0.65**	**−0.66**	**−0.69**	**−0.69**	−0.63		**−0.18**				**−0.49**		**−0.50**	**−0.56**		**−0.59**		
N2, $\alpha-\beta$											−0.10		−0.16	0.03		**0.002**		
charge											**−0.17**		**−0.17**	**−0.01**		**+0.19**		
μ_2-S	**−0.25**				**−0.26**		**−0.30**				**−0.25**			**−0.25**		**−0.26**		**−0.23**
charge																		
H1							+0.02		−0.01									
							+0.02		**0.000**									
H2							+0.03		+0.003									
							+0.04		**+0.11**									
energy	**−13 470.528**				**−13 546.912**		**−13 548.637**		**−13 415.765**		**−13 600.993**			**−13 602.150**		**−13 603.276**		**−13 414.012**
			−13 469.917[b]															

[a] The numbering scheme follows that in Figure 1. [b] Data obtained from the optimized structure of **A** without the 3H$^+$ added to the μ_2-S ligands.

than the more appropriate trianion or pentaanion was chosen for **X** = N or O due to expected difficulties with highly charged clusters when the energy of the HOMO is positive, and thus not bound, and the likelihood of unreliable results and artifacts even upon convergence. The energy values of the HOMO of [**I-N**]$^{2-}$ of about +0.3 eV (using SVP basis) and +0.06 eV (using TZVP basis) are taken as acceptable upper limits. The *E*(HOMO) of the [**I-N**]$^{3-}$ trianion at +3 eV (TZVP) exceeds any reasonable boundary. The choice of the dianion is considered acceptable, in view of the extensive electron delocalization and a smearing-over of redox effects (see below) found with these clusters.

The structural similarities between the energy minimized structures of the [**I-X**]$^{2-}$ clusters (**X** = N, O) and the experimentally determined FeMo-cofactor structure support the proposal[4] that the light atom was always present within the Fe_6 cavity but not detected in the earlier structure determinations.

The results for [**I-N**]$^{2-}$, [**I-O**]$^{2-}$, and [**I-N-3H**]$^{2-}$ are presented in Tables 2−4. The structures with X = N or O as central light atoms show symmetric Fe−Fe and Fe−X distances. They range from 2.45 to 2.70 Å (2.50−2.63 for the Fe_6 cavity) and 1.9 to 2.0 Å for X = N and from 2.56 to 2.75 Å and 2.02 to 2.07 Å for X = O. An asymmetric structure for the Fe_6O unit with wide ranges in the Fe−O and Fe−Fe distances has been reported earlier.[6]

A DFT calculation on the two electron oxidized [**I-N-3H**]^0 shows (Tables 3−5) an optimized structure with structural features, charges, and spin densities very similar to those of [**I-N**]$^{2-}$ and [**I-N-3H**]$^{2-}$, again demonstrating the extensive electron delocalization in these clusters.

The minimized energy structures of [**I-N**]$^{2-}$, [**I-N-3H**]$^{2-}$, and [**I-N-3H**]^0 show by Mulliken population analyses (MPA) large negative charges for the central N atom (−0.69, −0.65, and −0.66) and very similar, small positive charges for the Fe atoms. These charges fall into two sets. The central Fe_6 group of atoms shows an average charge per Fe of +0.18 (range 0.17−0.23) for [**I-N**]$^{2-}$, +0.17 (range 0.13−0.22) for [**I-N-3H**]$^{2-}$, and +0.21 (range 0.13−0.25) for [**I-N-3H**]^0. These similarities make it difficult to electronically differentiate the Fe_6 cores in the three clusters. The peripheral seventh Fe atom (Fe(2′)) shows charges of 0.29, 0.31, and 0.27, respectively, for [**I-N**]$^{2-}$, [**I-N-3H**]$^{2-}$, and [**I-N-3H**]^0.

The charges on Fe(2′) in structures **A**, **B**, **E**, **F**, and **G** (Figures 3−5**)** with Cl$^-$ as terminal ligands average +0.31 (range 0.29−0.32). The charges with CH_3S^- as terminal ligands average at +0.26 (range 0.24−0.28). The larger positive charges found for the peripheral Fe(2′) in all clusters probably reflect the higher electronegativity of the Cl$^-$ ligand and ionicity in the Fe−Cl bond by comparison to Fe−S bonds.

The net spin densities in [**I-N**]$^{2-}$ and [**I-N-3H**]$^{2-}$ (Table 3) are very similar to those obtained previously[10] for the BS6 state in [**I**]$^{2-}$. As reported earlier[10] for [**I**]$^{2-}$, the clusters [**I-N**]$^{2-}$ and [**I-N-3H**]$^{2-}$ can be partitioned into $MoFe_3$ and Fe_4 subunits with $S = 2$ and $S = {}^7/_2$, respectively. Antiferromagnetic coupling between these two subclusters will result in net $S = {}^3/_2$ oxidation states. The spin densities in [**I-N**]$^{2-}$ and [**I-N-3H**]$^{2-}$ just as

Table 4. Interatomic Distances in the Energy Minimized Structures for the Mechanistic Intermediates Shown in Figure 3 and Derived from [**I-N-3H**]$^{2-}$ (**A**−**G**) and the Two Electron Oxidized [**I-N-3H**] (**A^0**−**G^0**) Clusters[a]

dist (Å)	A	A^0	A, No H$^+$	A$_{SCH3}$	B	B^0	C	C^0	D	D^0	E	E^0	E$_{SCH3}$	F	F^0	G	G^0	H
Fe4−Fe5	2.52	2.56	2.52	2.55	2.47	2.47	2.61	2.66	2.58	2.50	2.82	2.82	2.74	2.89	2.76	3.09	3.15	2.57
Fe5−Fe3	2.60	2.58	2.56	2.53	2.50	2.78	2.63	2.66	2.72	2.64	2.73	2.70	2.81	2.71	2.61	2.67	2.44	2.54
Fe3−Fe8′	**2.45**	**2.50**	**2.55**	**2.62**	**2.66**	**2.55**	**2.73**	**2.86**	**2.69**	**2.59**	**2.65**	**2.62**	**2.67**	**2.62**	**2.53**	**2.68**	**2.61**	**2.60**
Fe4−Fe7′	**2.60**	**2.60**	**2.57**	**2.50**	**2.57**	**2.53**	**2.73**	**2.74**	**2.48**	**2.42**	**2.67**	**2.68**	**2.65**	**2.63**	**2.51**	**2.75**	**2.65**	**2.58**
Fe3−Fe4	**2.57**	**2.58**	**2.56**	**2.53**	**2.54**	**2.43**	**2.55**	**2.57**	**2.64**	**2.64**	**2.55**	**2.58**	**2.56**	**2.52**	**2.44**	**2.55**	**2.57**	**2.44**
Fe7′−Fe8′	**2.49**	**2.48**	**2.65**	**2.54**	**2.52**	**2.52**	**2.70**	**2.61**	**2.69**	**2.62**	**2.57**	**2.60**	**2.57**	**2.64**	**2.59**	**2.57**	**2.56**	**2.47**
Fe6′−Fe8′	**2.51**	**2.49**	**2.65**	**2.57**	**2.54**	**2.55**	**2.77**	**2.57**	**2.51**	**2.58**	2.99	3.00	2.74	3.21	2.59	**2.86**	**2.70**	**2.44**
Fe6′−Fe7′	**2.55**	**2.53**	**2.59**	**2.54**	**2.52**	**2.51**	**2.61**	**2.63**	**2.65**	**2.67**	2.75	2.72	2.97	3.48	3.34	**3.29**	**3.40**	**2.46**
Fe2′−Fe6′	**2.66**	**2.65**	**2.65**	**2.65**	**2.66**	**2.64**	**2.57**	**2.55**	**2.63**	**2.65**	2.66	2.66	2.65	2.45	2.48	**2.47**	**2.45**	**2.70**
Fe2′−Fe7′	2.66	2.65	2.65	2.68	2.64	2.61	2.67	2.55	2.78	2.84	2.65	2.62	2.69	2.67	2.60	2.65	2.61	2.58
Fe2′−Fe8′	2.63	2.59	2.73	2.65	2.68	2.65	2.64	2.61	2.61	2.58	2.69	2.68	2.65	2.78	2.54	2.64	2.59	2.61
Mo−Fe5	2.70	2.72	2.78	2.69	2.69	2.82	2.65	2.68	2.68	2.72	2.69	2.71	2.70	2.68	2.68	2.55	2.58	2.68
Mo−Fe3	2.72	2.72	2.77	2.68	2.68	2.76	2.81	2.80	2.72	2.74	2.75	2.75	2.72	2.72	2.70	2.69	2.76	2.79
Mo−Fe4	2.66	2.70	2.77	2.71	2.68	2.71	2.67	2.74	2.68	2.68	2.73	2.76	2.75	2.75	2.70	2.80	2.80	2.70
N1−Fe3	1.99	1.98	1.93	1.97	2.23	2.27	4.48	4.18			2.03	2.00	2.00	2.00	1.97	2.00	2.07	
N1−Fe4	1.97	1.97	1.91	1.94	2.11	1.99	2.55	2.09			2.00	2.01	2.04	2.10	2.03	2.01	2.05	
N1−Fe7′	1.97	1.96	2.03	1.91	1.96	1.97	3.13	4.87			1.96	1.96	2.02	2.02	2.01	1.99	2.05	
N1−Fe8′	1.83	1.85	1.99	1.97	1.95	1.93	3.46	3.22			2.02	2.00	1.95	1.98	2.03	2.06	2.07	
N1−Fe6′	1.96	1.98	2.04	1.98	1.98	2.00	3.17	3.70					2.52		3.19	2.88	3.00	
N1−Fe5	1.97	1.98	1.91	1.97	1.98	1.98		3.37					2.46		2.09	2.91	2.88	
N2−Fe5											1.89	1.89	1.88	2.04				
N2−Fe6′											1.87	1.88	1.86	2.82				
N1−N2											1.33	1.33	1.34	1.44	1.45	1.43	1.47	
Fe5−Fe6′	2.65	2.64	2.57	2.66	3.20	3.15	4.79	4.79	3.13	3.01	3.69	3.69	3.67	4.82	5.16	4.88	5.39	2.56
H1−H2							1.86	1.97	1.99	2.22								
Fe$_N$−H(1)																		
mean							1.89, 2.01		1.80, 1.80									
range							1.66−2.32		1.71−1.98									
							1.80−2.75		1.72−1.93									
Fe$_N$−H(2)																		
mean							1.74, 2.11		1.76, 2.07									
range							1.65−1.83		1.65−1.92									
							1.71−3.24		1.69−2.96									

[a] The numbering scheme follows that in Figure 1.

Table 5. Interatomic Distances for [**I-N-3H**]$^{2-}$ and the Two Electron Oxidized [**I-N-3H**] Clusters

distances (Å)[a]	exp. FeMoco[b]	[**I-N-3H**][c]	[**I-N-3H**][d]	[**I-N-3H**]$^{2-}$ [d]
Fe$_{6',7',8'}$−X	1.98(5)	2.07(10)	1.93(5)	1.92(5)
Fe$_{3,4,5}$−X	2.02(4)	1.98(1)	1.98(1)	1.97(5)
Fe$_{6',7',8'}$−Fe$_{2'}$	2.67(1)	2.69(1)	2.63(2)	2.65(1)
Fe$_{6',7',8'}$−Fe$_{6',7',8'}$	2.65(1)	2.59(2)	2.50(2)	2.52(2)
Fe$_{6',7',8'}$−Fe$_{3,4,5}$	2.59(2)	2.70(9)	2.58(5)	2.57(7)
Fe$_{3,4,5}$−Fe$_{3,4,5}$	2.61(2)	2.65(6)	2.57(1)	2.56(3)
Mo−Fe$_{3,4,5}$	2.69(2)	2.76(3)	2.71(1)	2.69(2)

[a] The numbering scheme follows that of Figure 1. [b] Reference 4. [c] Reference 5. [d] This work.

found[10] in [**I**]$^{2-}$ are much less than either five or four. This has been attributed previously to a "loss" of spin density to either "metal−ligand covalency or metal−metal interaction effects".

A Mechanism. Steps of the catalytic cycle (Figures 3−5) were calculated starting with either of two possible states for the cofactor, and the same charge was maintained throughout (by addition of equal numbers of H^+ and e^-) between steps.

The states were $[(Cl)Fe^{II}_6Fe^{III}Mo^{IV}S_9(H^+)_3N^{3-}(Gl)(Im)]^{2-}$, [**I-N-3H**]$^{2-}$, and $[(Cl)Fe^{II}_4Fe^{III}_3Mo^{IV}S_9(H^+)_3N^{3-}(Gl)(Im)]$, [**I-N-3H**]^0. These are the triply protonated ENDOR/ESEEM,[9] [**I-N**]$^{5-}$, and Mössbauer,[8] [**I-N**]$^{3-}$, models, respectively. The results are shown in Tables 3 and 4.

Addition of an H_2O ligand to Fe(5), lengthening of the Fe(5)−Fe(6′) distance in **A** (Figure 4A) **(**from 2.65 to 3.20 Å, Figure 4), and energy minimization converges to structure **B** (Figure 4B).

In the latter, the μ_2-SH ligand between Fe(5) and Fe(6′) has been converted to a terminal ligand on Fe(6′). The mean Fe−Fe distance between the Fe$_{3,4,7',8'}$ base atoms in the Fe$_6$ center is 2.57(4) Å, and the mean Fe$_{3,4,7'8'}$−N(1) distance is 2.06(8) Å. The charge on the central N atom is −0.63 and nearly indistinguishable from the charge of the N atom in **A** (−0.65).

Addition of three electrons to **B** and three protons (on the central N atom) gives after structure optimization **C** (Figure 4C). In **C**, the Fe(5)−Fe(6′) distance has now increased to 4.79 Å, and the ammonia molecule that forms serves as a terminal ligand to Fe(4) (Fe(4)−NH_3 = 2.55 Å).

Not unexpectedly, the two electron oxidized cluster, **C^0**, shows the Fe(4)−NH_3 distance at 2.09 Å (Table 4). In **C**, the hydrogen atoms, originally on the two μ_2-SH ligands in **B**, have the option either to occupy the corners of the two cuboidal subunits or to be associated with the μ_2-S atoms. At convergence, the former option was found preferable at an H−H distance of 1.86 Å. The mean Fe−H distance in **C** is 1.82(11) Å. The oxidized **C^0** cluster shows the H atoms in nearly the same positions with an H−H distance of 1.97 Å and a mean Fe−H distance of 1.76(2) Å. The MPA charges of the hydrogen atoms in **C** are positive but very small at +0.02 and +0.04. At this stage, it is difficult to formally describe them as either μ_3-H hydrogen atoms or μ_3-H^- hydride ligands.

The removal of NH_3 and H_2O from **C** followed by structure optimization results in **D** (Figure 5D). In **D**, the Fe(5)−Fe(6′) distance is shortened to 3.13 Å, the bridging mode of the SH ligand is re-established, and the two H atoms in the Fe$_6$ cavity, each interacting with four Fe atoms, show an H−H distance of 1.99 Å and a mean Fe−H distance of 1.78(4) Å.

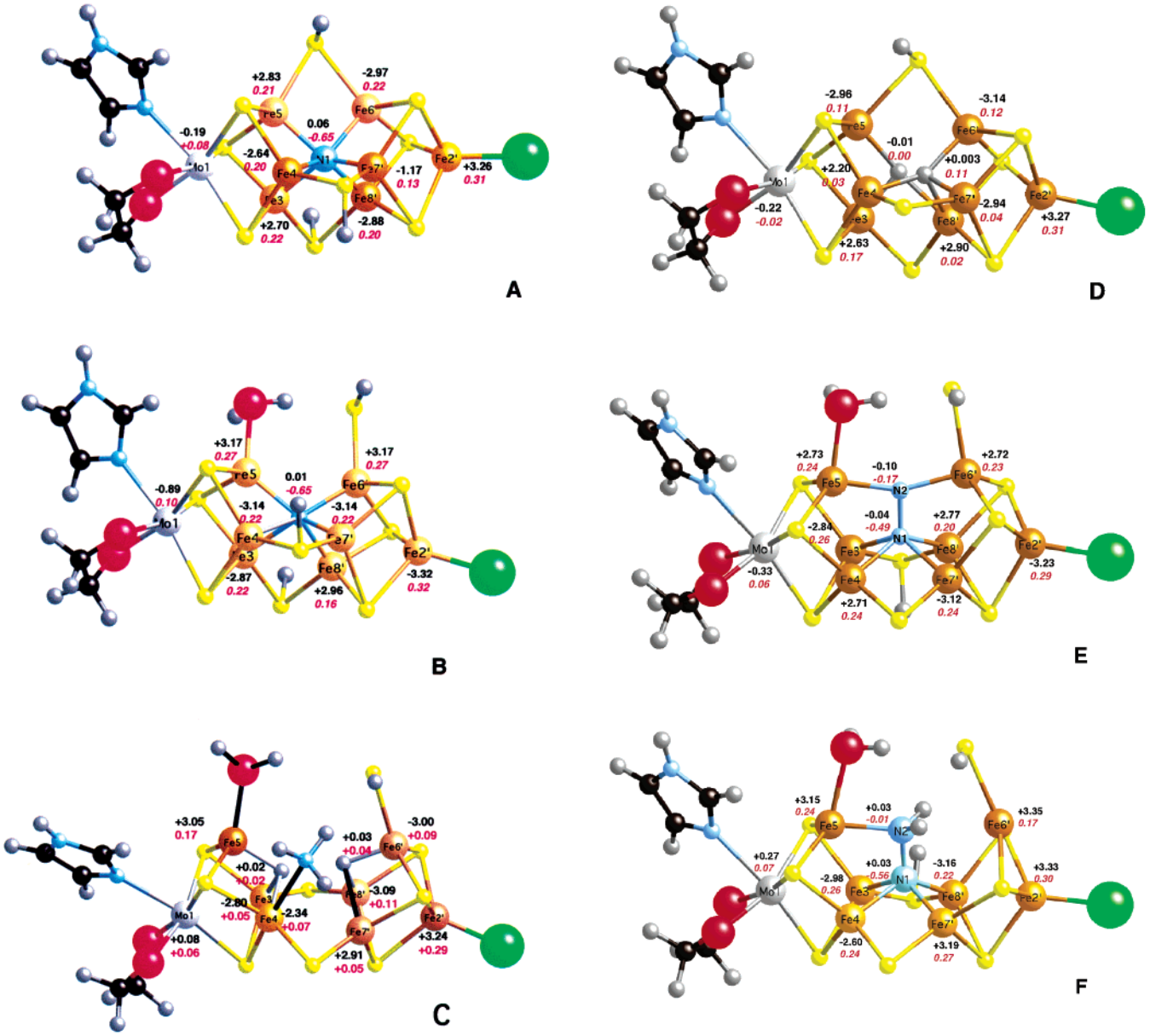

Figure 4. Energy minimized structures of the triprotonated form of the $[(Cys)Fe^{II}_6Fe^{III}Mo^{IV}S_9(N)(h\text{-}citr)(His)]^{n-}$ anion, $n = 5$ [**I-N-3H**]$^{2-}$, **A**; the aquation derivative of **A** $[(Cys)Fe^{II}_6Fe^{III}Mo^{IV}S_9(N)(H_2O)(H^+)_3(h\text{-}citr)(His)]^{n-}$ ($n = 2$, **B**) and $[(Cys)Fe^{II}_6Fe^{III}Mo^{IV}S_9(NH_3)(H_2O)(H^+)_3(h\text{-}citr)(His)]^{n-}$ ($n = 2$, **C**) obtained upon addition of $3e^-$ and $3H^+$ to **B**. These structures are nearly identical to those of the two electron oxidized analogues $\mathbf{A^0}$, $\mathbf{B^0}$, and $\mathbf{C^0}$. The pair of numbers adjacent to the individual atoms represents the electronic spin vectors, $\alpha-\beta$, on top and the MPA charges on the bottom.

Similar interactions are found in $\mathbf{D^0}$ with H−H distances of 2.22 Å and mean Fe−H distances of 1.79(3) Å. In **D**, the charges on the H atoms are 0.00 and +0.10. As is the case with **C** and $\mathbf{C^0}$, it is difficult to formally describe the hydrogens as either H atoms or μ_3-H^- ligands. The minimum energy, optimized structure of **D** is 14 kJ/mol higher in energy than **H** with three protons on the μ_2-S atoms, **H**-3H.

Addition of an electron and a proton to **D**, followed by addition of H_2O and formal replacement of H_2 by N_2, gives, after structure optimization, **E** (Figure 5E).

In **E**, the N_2 molecule is inserted into the Fe_6 cavity which now shows the Fe(5)−Fe(6′) distance at 3.69 Å. The mean Fe−Fe distance between the remaining four Fe atoms in the Fe_6

Figure 5. Energy minimized structure of $[(Cys)Fe^{II}_6Fe^{III}Mo^{IV}S_9(H^+)_3(h\text{-}citr)(His)]^{n-}$ ($n = 2$, **D**) obtained following release of NH_3 and H_2O from **C**; of $[(Cys)Fe^{II}_6Fe^{III}Mo^{IV}S_9(N_2)(H^+)_2(H_2O)(h\text{-}citr)(His)]^{n-}$ ($n = 2$, **E**) obtained following aquation, replacement of H_2 by N_2, and addition of 1H to **D**; of $[(Cys)Fe^{II}_6Fe^{III}Mo^{IV}S_9(NNH_2)(H^+)_2(H_2O)(h\text{-}citr)(His)]^{n-}$ ($n = 2$, **F**) obtained following the addition of two electrons and two protons to **E**; and of $[(Cys)Fe^{II}_6Fe^{III}Mo^{IV}S_9(NNH_3)(H^+)_3(H_2O)(h\text{-}citr)(His)]^{n-}$ ($n = 2$, **G**) obtained following the addition of two electrons and two protons to **F**.

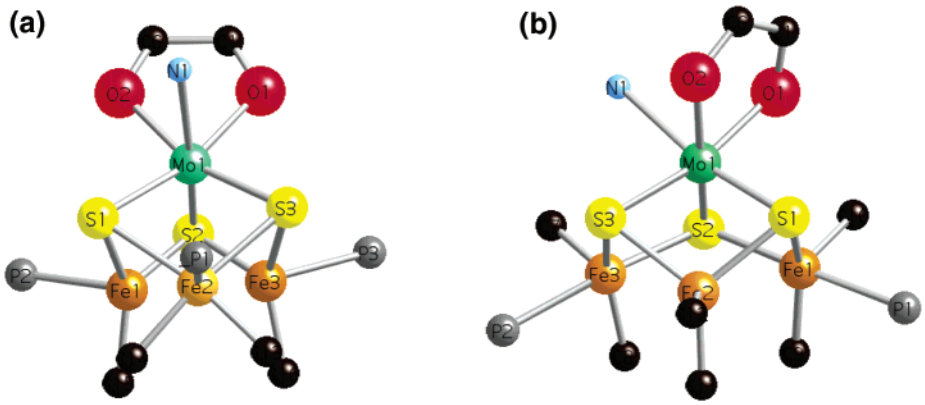

Figure 6. Crystal structures of the (a) [(Cl_4-cat)Mo(py)$Fe_3S_3(CO)_4(P^nPr_3)_3$] and (b) [(Cl_4-cat)Mo(py)$Fe_3S_3(CO)_6(P^nPr_3)_2$] clusters. For clarity, only the carbon atoms attached to the oxygen donors of the catecholate ligands are shown. Also hidden are the alkyl groups of the PR_3 ligands, the oxygen atoms of the carbonyl ligands, and the carbon atoms of the Mo-coordinated pyridine ligands.

center is 2.62(3) Å. The N_2 molecule, in the center of the Fe_6 cage, is oriented perpendicular to the square of Fe_3, Fe_4, $Fe_{7'}$, and $Fe_{8'}$ and is asymmetrically bound to all six Fe atoms. The Fe(5) and Fe(6′) distances from N(2) are 1.89 and 1.87 Å and are shorter than the $Fe_{3,4,7',8'}$−N(1) distances that average 2.00(2) Å. The "activated", reduced, N_2 molecule shows charges of −0.49 and −0.17 at N(1) and N(2), respectively, and a long N−N distance of 1.33 Å.

Two electron reduction of **E** and addition of $2H^+$ to the N_2 molecule after optimization gives **F** (Figure 5F). It contains a coordinated isodiazene molecule with charges of −0.56 on N(1) and −0.01 on N(2). The N−N distance is 1.44 Å, and the N(2) atom is now bound only to Fe(5) at a distance of 2.04 Å. The $Fe_{3,4,7',8'}$−N(1) distances average 2.02(3) Å.

An additional $2e^-$, $2H^+$ addition to **F** and energy minimization gives **G** (Figure 5G). In the optimized structure of **G**, the Fe(5)−Fe(6′) distance is 4.88 Å. The coordinated isohydrazide molecule in **G** shows charges of −0.59 and +0.19 for N(1) and N(2), respectively, with a N−N distance of 1.43 Å apparently ready for cleavage of the N−N bond. The $Fe_{3,4,7',8'}$−N(1) distances average at 2.01(2) Å. The mean Fe−Fe distance between the $Fe_{3,4,7',8'}$ base atoms in the Fe_6 center is 2.64(5) Å.

The removal of NH_3 and H_2O from **G** gives structure **A** with a centrally located N atom (charge = −0.65) and a mean Fe−Fe distance (in the Fe_6 cage) of 2.55(4) Å.

Discussion

Electronic Structure of the FeMo-Cofactor; M−M Interactions. The two oxidation levels of the FeMoco, [**I-N**] and $[\mathbf{I\text{-}N}]^{2-}$, originally assigned by Mössbauer[8] and EPR/ENDOR[9] spectroscopy, contain the $Mo^{IV}Fe^{III}_3Fe^{II}_4S_9N$ and $Mo^{IV}Fe^{III}$-$Fe^{II}_6S_9N$, respectively.

The total number of valence electrons (including the terminal and central atoms) in [**I-N**] and $[\mathbf{I\text{-}N}]^{2-}$ are 103 and 105. These correspond to ∼13 e^-/M, and, by conventional electron counting rules,[33] [**I-N**] and $[\mathbf{I\text{-}N}]^{2-}$ are electron deficient. Electron deficiency of this magnitude in organometallic clusters usually is reflected in short M−M distances interpreted as M−M bonding. The N^{3-} void FeMoco structures [**I**] and $[\mathbf{I}]^{2-}$ are even more electron deficient, each by eight electrons. The calculated very short Fe−Fe and Fe−Mo distances in [**I**][10] and $[\mathbf{I}]^{2-}$ (Table 4) are consistent with extensive M−M interactions. These interactions are significant but may not be essential for the stability of [**I**] where Fe−Fe bonding is proposed to be inherently weak.[10]

Recent DFT studies of the bonding in model compounds, containing the $[MoFe_3S_3]^{2+}$ cores, are in agreement with this assessment.[13] A theoretical analysis of the electronic structure and bonding in a series of Roussin-type[34] clusters with the $[MoFe_3S_3]^{2+}$ cores (Figure 6) shows significant lengthening or shortening of M−M distances as a result of electron gain or loss.[13,35]

The effects on M−M distances of S substitution by either Se or Te in the $[MoFe_3S_3]^{2+}$ [13] or $[M_6E_8(CO)_6]$ clusters[36] have been examined. The lack of significant changes of the short M−M distances in these clusters has been interpreted as indication of (relatively weak) intermetallic bonding.

Supporting evidence that M−M attractive interactions are operative in the FeMo-cofactor is provided by similar calculations where the S^{2-} ligands are replaced by Se^{2-}. DFT calculations and energy minimization of the center-voided FeMoco, $[\mathbf{I}]^{2-}$, and also of the same cluster with Se^{2-} ligands in place of S^{2-} show the $Mo^{IV}Fe^{III}Fe^{II}_6Se_9$ cores with virtually identical Fe−Fe distances (Table 2).

The structural similarities between the $MoFe_3S_3$ cores in the model clusters and the core in the Mo-containing cuboidal subunit of the FeMo-cofactor are apparent. The redox-induced structural flexibility of the model $MoFe_3S_3$ clusters has led to the suggestion[12] that, following reduction, the cofactor may also distort (expand) in a manner that facilitates the dinitrogen fixation process (vide infra).

The apparent "plasticity"[6] of the cofactor and its inherent ability to undergo distortions have also been identified previously[22a] as characteristics important in N_2 binding and activation. The delocalization of charge in the FeMo-cofactor also has prompted Dance to suggest[19b] that the Fe_6 unit may be regarded as an electron reservoir where all iron atoms are involved in the cooperative binding and activation of substrates.

(33) Michael, D.; Mingos, P.; May, A. S. Structure and Bonding Aspects of Metal Cluster Chemistry. In *Chemistry of Metal Cluster Complexes*; Shriver, D. F., Kaesz, H. D., Adams, R. D, Eds.; VCH: New York, 1990; Chapter 2, pp 81.

(34) Roussin, M. L. *Ann. Chim. Phys.* **1858**, *52*, 285.

(35) In these calculations, however, the ground states which show some very short Fe−Fe distances lie very close in energy (∼10 kJ) to excited states, where the same Fe−Fe distances are longer by as much as 0.8 Å. This is a clear indication of weak M−M bonding and inherent structural flexibility.

(36) Fan, P.-D.; Deglmann, P.; Ahlrichs, R. *Chem.-Eur. J.* **2002**, *8*, 1059.

Table 6. Energy Correlations between the Mechanistic Intermediates Shown in Figure 3 and Derived from [**I-N-3H**]$^{2-}$ (**A** → **G**) and [**I-N-3H**]^{0} (**A^0** → **G^0**) Clusters[a]

$E_B = -13\,546.912$	$E_A + E_{H2O} = -13\,546.892$	$\Delta E_{A\rightarrow B} = -53$ kJ/mol
$E_{B0} = -13\,546.800$	$E_{A0} + E_{H2O} = -13\,546.798$	$\Delta E_{A0\rightarrow B0} = -5.3$ kJ/mol
$E_C = -13\,548.637$	$E_A + E_{1.5H2} + E_{H2O} = -13\,548.650$	$\Delta E_{A\rightarrow C} = +34$ kJ/mol
$E_{C0} = -13\,548.551$	$E_{A0} + E_{1.5H2} + E_{H2O} = -13\,548.556$	$\Delta E_{A0\rightarrow C0} = +13$ kJ/mol
$E_D = -13\,415.765$	$E_C - E_{NH3} - E_{H2O} = -13\,415.761$	$\Delta E_{C\rightarrow D} = -11$ kJ/mol
$E_{D0} = -13\,415.640$	$E_{C0} - E_{NH3} - E_{H2O} = -13\,415.675$	$\Delta E_{C0\rightarrow D0} = -92$ kJ/mol
$E_E = -13\,600.993$	$E_D - E_{0.5H2} + E_{N2} + E_{H2O} = -13\,600.992$	$\Delta E_{D\rightarrow E} = -2.6$ kJ/mol
$E_{E0} = -13\,600.882$	$E_{D0} - E_{0.5H2} + E_{N2} + E_{H2O} = -13\,600.867$	$\Delta E_{D0\rightarrow E0} = -39.4$ kJ/mol
	$E_H + E_{N2} + E_{H2} + E_{H2O} = -13\,600.997$	$\Delta E_{H\rightarrow E} = +11$ kJ/mol
	$E_{H0} + E_{N2} + E_{H2} + E_{H2O} = -13\,600.863$	$\Delta E_{H0\rightarrow E0} = -50$ kJ/mol
$E_F = -13\,602.150$	$E_E + E_{H2} = -13\,602.165$	$\Delta E_{E\rightarrow F} = +39$ kJ/mol
$E_{F0} = -13\,602.051$	$E_{E0} + E_{H2} = -13\,602.054$	$\Delta E_{E0\rightarrow F0} = +8$ kJ/mol
$E_G = -13\,603.276$	$E_F + E_{H2} = -13\,603.322$	$\Delta E_{F\rightarrow G} = +121$ kJ/mol
$E_{G0} = -13\,603.188$	$E_{F0} + E_{H2} = -13\,603.223$	$\Delta E_{F0\rightarrow G0} = +92$ kJ/mol
$E_A = -13\,470.528$	$E_G - E_{NH3} - E_{H2O} = -13\,470.400$	$\Delta E_{G\rightarrow A} = -336$ kJ/mol
$E_{A0} = -13\,470.528$	$E_{G0} - E_{NH3} - E_{H2O} = -13\,470.312$	$\Delta E_{G0\rightarrow A0} = -320$ kJ/mol
$E_H = -13\,414.012$	$E_D - E_{1.5H2} = -13\,414.007$	$\Delta E_{D\rightarrow H} = -13$ kJ/mol
$E_{H0} = -13\,413.876$	$E_{D0} - E_{1.5H2} = -13\,413.882$	$\Delta E_{D0\rightarrow H0} = +10$ kJ/mol
$E_{N2} = -109.449$		
$E_{H2O} = -76.364$		
$E_{NH3} = -56.512$		
$E_{H2} = -1.172$		

[a] Energies are in hartrees, H; 1 H = 2626 kJ = 627.5 kcal.

In concert with the results of a previous study,[10] our calculations on various forms of the cofactor show a slight lengthening of the average M−M distances upon reduction (Table 4). These observations are consistent with M−M attractive interactions in the electron-deficient states but differ from the original EXAFS data[37] which show a slight shortening upon reduction.

In the previously reported, extended spin-polarized broken-symmetry DFT calculation,[10] the minimum energies and optimized structures of the $Mo^{IV}Fe^{II}_6Fe^{III}$, $S = {}^3/_2$ oxidation state ([**I**]$^{2-}$) with various spin coupling patterns were obtained. The most likely broken-symmetry state was considered to be one with a $MoFe_3$ cluster with $S = 2$ antiferromagnetically coupled to an Fe_4 cluster with $S = {}^7/_2$. Similar calculations with the $Mo^{IV}Fe^{II}_4Fe^{III}_3$, $S = {}^3/_2$ oxidation state ([**I**]) gave results in poorer agreement with experiment. Our calculations with [**I-N**]$^{2-}$ and [**I-N-3H**]$^{2-}$ show spin densities on the Fe atoms (Table 3) with possible coupling patterns similar to those reported for [**I**]$^{2-}$.[10]

The Central Light Atom. After consideration of O and N as possible candidates, Dance[6] and Hinnemann and Nørskov[5] proposed N as the most likely central light atom in a $Mo^{IV}Fe^{III}_3Fe^{II}_4S_9(\mu_6\text{-}N^{3-})$ core[6] and a protonated $Mo^{IV}Fe^{III}_3Fe^{II}_4S_9(\mu_6\text{-}N^{3-})(H^+)_3$ analogue.[5] In this latter study, protonation of the [**I-X**]$^{5-}$ pentaanion by three protons was applied in an effort to reduce the excessive negative charge and possible computational problems associated with it.[5]

In a more recent study[7] of the [**I**−**X**]$^{5-}$ cofactor using a spin-polarized, broken symmetry DFT calculation such as the one previously used[10] with [**I**]$^{2-}$, the central atom **X** was identified as N^{3-}. In the same calculation, successful matching of the calculated redox potentials to those experimentally determined was achieved using the $Mo^{IV}Fe^{III}_3Fe^{II}_4S_9(\mu_6\text{-}N^{3-})$ description of the cofactor core.

The results of comparative DFT calculations on [**I-X-3H**]$^{2-}$ and [**I**]$^{2-}$ reported herein for **X** = N, O (Table 2) agree with the consensus conclusion that the light atom in the FeMo-cofactor is N. It should be pointed out, however, that the results are not as clearly in favor of N as previously suggested.[5,6,10] We tentatively assign X as N on the basis of the marginally closer proximity of the calculated structures (Table 2) to those experimentally determined for the FeMo-cofactor.

The mean charge for the Fe_6 atoms in [**I**]$^{2-}$ is 0.11 and considerably smaller than the corresponding value (0.23) in [**I-N-3H**]$^{2-}$. The results show that, as suggested previously,[10] the electronic description of the metals in [**I**]$^{2-}$, without a central light atom, is best described in terms of a reduced $Mo^{IV}Fe^{III}\text{-}Fe^{II}_6$ core. The calculations indicate that the EPR model is consistent with the [**I**]$^{2-}$ state and the Mössbauer model is consistent with the [**I-N**]$^{2-}$ or [**I-N-3H**]$^{2-}$ states. It is quite clear that the N atom introduced to [**I**]$^{2-}$ undergoes internal reduction and the Fe atoms in [**I-N**]$^{2-}$ are oxidized. The total minimum energy of [**I**]$^{2-}$ (E_H, Table 6) was found to be higher by only ~10 kJ/mol than that of [**I-N-3H**]$^{2-}$ − NH_3 ($E_A - E_{NH3}$). This imperceptibly small difference indicates that the center-voided

(37) Christiansen, J.; Tittsworth, R. J.; Hales, B. J.; Cramer, S. P. *J. Am. Chem. Soc.* **1995**, *117*, 10017.

form of the cofactor is inherently stable and energetically accessible at least in the $[\mathbf{I}]^{2-}$ state.

The lack of significant differences in the atomic charges of the metal atoms in the calculations ($[\mathbf{I\text{-}N}]^{2-}$ vs $[\mathbf{I\text{-}N\text{-}3H}]^{2-}$) indicates that internal oxidation within the cofactor that results in N^{3-} formation is a process "smeared-over" an extensively delocalized system. A comparison of the calculated structural data for $[\mathbf{I\text{-}N}]^{2-}$, $[\mathbf{I\text{-}N\text{-}3H}]^{2-}$, $[\mathbf{I\text{-}N\text{-}3H}]^{0}$, and the experimental structure of the FeMo-cofactor [4] (Table 5) demonstrates the similarities between all of these structures.

The shorter M−M distances and apparently greater attractive M−M interactions in $[\mathbf{I}]^{2-}$ by comparison to $[\mathbf{I\text{-}N}]^{2-}$, $[\mathbf{I\text{-}N\text{-}3H}]^{2-}$, or $[\mathbf{I\text{-}N\text{-}3H}]^{0}$ are not unexpected considering that the former cluster is deficient by the valence electrons of the central N atom.

Origin of the Central Atom. The presence of the N atom in the center of the Fe_6 prism has raised[5] two important but as yet unresolved issues. These are centered on the following questions: (a) is the central nitrogen atom an active remnant of the N_2 fixation process or (b) is it simply a nonparticipating spectator that serves as a cofactor structure stabilizing feature? Both affirmative and negative answers to the first question have been offered.

The placement of the central N atom in the cofactor, as a structure stabilizing feature, and apparently a spectator species as far as N_2 reduction is concerned, has been described.[6] It is generated following reduction and protonation to NH_3 of one of the N atoms of a N_2 molecule. The latter is adsorbed above one of the Fe_4S_4 faces of the empty form of the FeMo-cofactor. After N−N bond cleavage and liberation of NH_3, the other N atom "falls" in the center of the Fe_6 cavity. We attempted a calculation with N_2 placed above a four iron face of the Fe_6 prism using DFT with a nonhybrid functional similar to that used previously.[6] We could not obtain a minimum; however, it is clear that **E** lies at least 100 kJ/mol lower in energy.

A different view regarding the central N atom has been presented in a recent ESEEM/ENDOR spectroscopic study on the nitrogenase FeMoS center.[38] In this study, two new weak absorptions were detected and assigned to the central N atom. These absorptions did not show isotopic shifts when isotopically labeled dinitrogen (^{15}N) was used as a substrate. These results were considered evidence that the central nitrogen in the FeMoS cluster is not exchangeable and it is not there as a consequence of the nitrogen fixation process. This conclusion was based on the assumption that spin coupling with the central nitrogen is sufficiently strong to be detectable. It does not consider the possibility that the observed signals are due to other, nonexchangeable, protein nitrogen atoms in the proximity of the cofactor (not previously found by less sensitive measurements). The results are thought provoking but "not 100% interpretable".[39]

We propose a mechanism for nitrogen fixation (Figure 3) that considers the central atom in the cofactor as an exchangeable nitrogen. This premise may appear controversial in view of the ESEEM/ENDOR results described above. It is our position, however, that there exist questions regarding the spectroscopic detectability of the central N atom that remain to be answered. Such questions originally were raised by Lovell et al.[7] in their calculations of $[\mathbf{I}]^{5-}$, where the very small spin population at the N^{3-} center ($\sim -0.02e^-$) suggests that a ^{14}N (or ^{15}N) hyperfine signal may be "difficult to observe or identify". An examination of the environment around the cofactor shows hydrogen-bonding interactions with a multitude of amino acids that include arginines 96, 359; glycines 356, 357; histidine 195; and leucine 358. This relatively nitrogen-rich environment may also be a source of weak ^{14}N signals from nonexchangeable N atoms and a possible source of spectroscopic interference as well. Our results show (Table 3) a very small spin population of the N^{3-} center in $[\mathbf{I\text{-}N\text{-}H}]^{2-}$ at $0.06e^-$, and the same cautions apply. There is a clear need for further evaluations of an alternative account for the central N atom and its possible association with the N_2 fixation process.

A Proposed Mechanism. Mechanistic aspects of N_2 activation and reduction by nitrogenase have been proposed previously on the basis of kinetic studies, theoretical calculations, or specific properties and comparisons with model complexes.

Extensive kinetic studies have led Thorneley and Lowe[40] to propose a catalytic cycle where the transfer of eight electrons and eight protons (in eight steps; E_0−E_7) to one-half of the MoFe protein of nitrogenase results in the reduction of one N_2 molecule and two H^+ (eq 1).

$$N_2 + 8H^+ + 8e^- \rightarrow 2NH_3 + H_2 \qquad (1)$$

Briefly, in the Thorneley−Lowe mechanism, the MoFe protein binds N_2 after a three or four electron reduction below the dithionite reduced resting state, and formation of H_2 occurs only after at least two H^+ and two electrons have been added to the protein.

Quenching by acid or base release hydrazine, and H_2 is released upon acidification. In addition to other important details of catalytic function, the kinetic data also support (a) N_2 binding to the FeMo-cofactor concomitant with H_2 release and (b) H_2 inhibition of ammonia synthesis. At present, molecular descriptions of the activation and reduction of N_2 by the FeMo-cofactor are subject to the constraints imposed by the Thorneley−Lowe kinetic studies and mechanistic scheme.

Various proposed mechanisms exist that are based on either specific structural features and sites of the FeMo-cofactor or on complexes that have shown reactivity properties relevant to nitrogenase action. Mechanisms of FeMoco-catalyzed N_2 reduction have considered the Fe_6, Fe_6N, or Mo structural subunits as possible sites for N_2 activation and reduction. Theoretical studies that place emphasis on open faces of the cofactor as sites for N_2 binding have been discussed in considerable detail by Deng and Hoffmann,[17] Dance,[19c] and Rod et al.[22b,c] In three of these reports,[19c,22b,c] the "on-top" binding of N_2 to a single Fe atom has been reported to be most stable. A possible model for the insertion of N in the center of the FeMo-cofactor also has been suggested.[41]

The mechanism proposed in this paper (Figure 3) explores the possibilities that (a) distortions facilitate interactions of the Fe_6 central unit of the cofactor with N_2 and derivative substrates,

(38) Lee, H.-I.; Benton, P. M. C.; Laryukhin, M.; Igarashi, R. Y.; Dean, D. R.; Seefeldt, L. C.; Hoffman, B. M. *J. Am. Chem. Soc.* **2003**, *125*, 5604.
(39) Britt, D. University of California, Davis, CA, personal communication.
(40) Thorneley, R. N. F.; Lowe, D. J. *J. Biol. Inorg. Chem.* **1996**, *1*, 576.
(41) (a) Sellman, D.; Utz, J.; Blum, N.; Heinemann, F. *Coord. Chem. Rev.* **1999**, *190*, 602. (b) Sellmann, D.; Sutter, J. *J. Biol. Inorg. Chem.* **1996**, *1*, 587. (c) Sellman, D.; Fursattel, A.; Sutter, J. *Coord. Chem. Rev.* **2000**, *200*, *200*, 545.

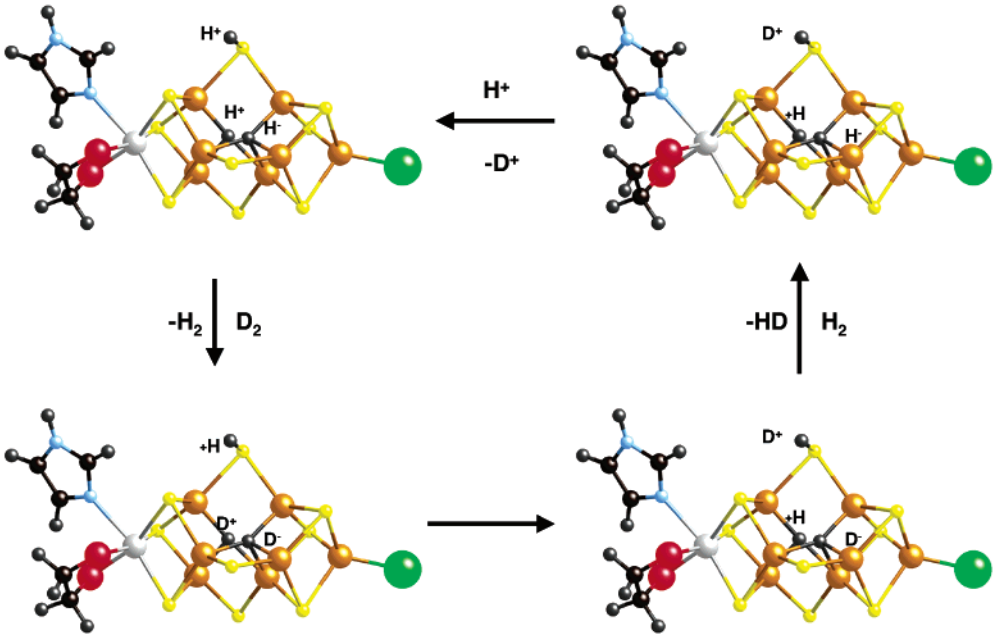

Figure 7. A possible mechanism for HD exchange, based on the $[(Cys)Fe^{II}_6Fe^{III}Mo^{IV}S_9(H^+)_3(h\text{-}citr)(His)]^{n-}$ clusters ($n = 0$, $\mathbf{D^0}$ or $n = 2$, **D**).

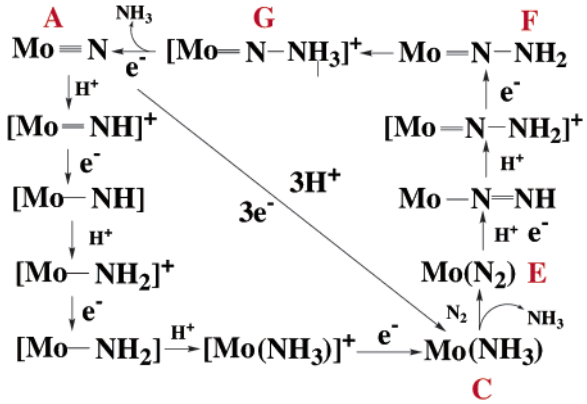

Figure 8. A mechanism for the catalytic reduction of N_2 by the $(HIPTN_3)$-MoN_2 complex[15] ($HIPTN_3$ = the hexaisopropyl terphenyl derivative of triethylene tetramine). Intermediates with common reduced N_2 derivatives to intermediates shown in Figure 3 are labeled by the corresponding letter labels in Figure 3.

(b) the central atom in the cofactor is an exchangeable nitrogen, and (c) the individual steps are related by H^+/e^- additions (and reduction of substrate; Figure 3, steps **B** → **C**; **D** → **E**; **E** → **F**; **F** → **G**) or ligation/deligation (and distortion of the Fe_6 center).

Addition of a water molecule to an Fe atom within one of the Fe−μ_2-S−Fe units in the cofactor results in the conversion of the −μ_2-SH into a terminally coordinated SH ligand on the second Fe atom (Figure 3, steps **A** → **B**; **D** → **E**) and a lengthening of the particular Fe−Fe distance in structures such as **B** and **E**. The change that eventually leads to **B** or **E** is probably hindered by only a small energy barrier. Indeed, synthetic MoFeS clusters are available[42] which contain $MoFe_3S_3$ cuboidal subunits bridged by two −μ_2-S ligands. The cores of these clusters resemble those of **B** or **E** (Figures 5 and 8) and contain a long Fe−Fe distance (~4.45 Å) and a distorted −μ_6-S ligand in place of the N^{3-} and N_2 ligands in **B** and **E**, respectively.

(42) (a) Holm, R. H.; Zhang, Y. G. *J. Am. Chem. Soc.* **2003**, *125*, 11 and references therein. (b) Koutmos, M.; Coucouvanis, D., work in progress.

Dissociation of the water ligand from the Fe(5) atoms in **B** and **E** results in the regeneration of the −μ_2-SH bridge and shortening of the Fe−Fe distance (Figure 3, steps **G** → **A**; **C** → **D**).

Water was chosen as a two electron donor to Fe(5) to facilitate Fe−Fe bond breaking and elongation of the Fe(5)−Fe(6′) distance. In the protein, amino acid functional groups such as the proximal imidazole group of histidine 195 could be envisioned as possible local two electron donors. One can only speculate regarding the activation of **A** and formation of **B**. Protein conformation changes that may accompany electron or proton transfers could assist in lowering the activation energy necessary for coordination of a ligand (water or imidazole) to Fe(5) and start the conversion of **A** to **B** and the catalytic cycle.

This speculation finds some support in the extensive structural distortions (and a change in the coordination sphere of one of the Fe atoms) observed with the **P** clusters of the MoFe protein[3] of nitrogenase in oxidation levels that differ by only two electrons.

The sequence of catalytic steps can start with the cofactor as is known from the latest structure determination[4] and in this study assumed to be a stable intermediate. Calculations were carried out with both the protonated EPR/ESEEM model,[9] [**I-N-3H**]$^{2-}$, and the protonated Mössbauer model,[8] [**I-N-3H**]^0. The results of these calculations (Tables 3 and 4) and the optimized structures (Figures 4 and 5) are surprisingly similar in both interatomic distances and individual atomic charges. Extensive delocalization does not allow for a differentiation between the two descriptions of **I-N** that differ by two electrons. The charges on the Fe atoms, in particular, do not reveal identifiable differences in oxidation states, and the charges on the nitrogen substrates are nearly indistinguishable (Table 3). As stated previously, the protons were added to neutralize part or all of the charge, in [**I-N**]$^{5-}$ and [**I-N**]$^{3-}$, and more importantly to participate in the N_2 fixation process. Arguably, it is not unrealistic to expect H^+ attached as counterions to either a pentaanionic or a trianionic cluster at some stage during turnover considering the high flux of protons. As pointed out previously,

the FeMo-cofactor and surroundings must be "loaded with protons" prior to N_2 fixation.[22c]

The basic μ_2-S^{2-} ligands were chosen as the most likely protonation sites. Previous DFT calculations have shown[10,22c] that a single H atom binds more strongly to μ_2-S^{2-} than either Fe or μ_3-S^{2-} sites. In a study of the three electron reduction of the $[Fe_3S_4]^+$ cluster of *A. vinelandii* ferredoxin I, it was determined[43] that after the addition of the first electron, a proton had to be added before addition of the second electron. Evidence was presented that the proton transfer was directly on the $[Fe_3S_4]^0$ cluster, most likely on a μ_3-S^{2-} site. This result was considered[44] relevant for the function of the FeMo-cofactor site in nitrogenase where it was suggested that sequential electron/proton transfer may use the three μ_2-S^{2-} ligands in the cofactor as likely protonation sites. In [**I-N-3H**]$^{2-}$, **A** (Figure 4A), and [**I-N**]$^{2-}$, the N^{3-} central atoms are symmetrically bound in a μ_6 fashion by the six Fe atoms of the Fe_6 "cage". The Fe$-\mu_2$-SH and Fe$-\mu_2$-S distances, respectively, show significant differences. As expected, and also reported previously,[7] the Fe$-\mu_2$-SH distances in [**I-N-3H**]$^{2-}$ (mean 2.36(4) Å; range 2.30−2.41 Å) and [**I-N-3H**]^0 (mean 2.33(3) Å; range 2.27−2.37 Å) are longer by ∼0.15 Å than the Fe$-\mu_2$-S distances in [**I-N**]$^{2-}$. In the latest X-ray structure of the FeMo-cofactor,[4] the Fe$-\mu_2$-S bonds range from 2.17 to 2.26 Å with an average of 2.22 Å. Clearly in the resting state of the FeMo-cofactor, the $-\mu_2$-S ligands are not protonated. The optimized structure of [**I-N-3H**]$^{2-}$ with three H^+ attached one each to the three μ_2-S ligands has a lower total energy $E_A = -13\,470.528$ H,[45] as compared to −13 469.917 H for the unprotonated cluster, [**I-N**]$^{2-}$ (Tables 3 and 6).

The formation of ammonia from **A**, following the addition of three protons to the central N atom and three electrons to **A**, is preceded by the hydrolysis of the Fe(5)−Fe(6′) bond which breaks to give **B** and expose the central N atom for protonation.

In **C**, the energy minimized structure shows the NH_3 molecule weakly bound to Fe(4) (Fe(4)−NH_3, 2.55 Å).

The generation of NH_3 from the central N atom in the FeMo-cofactor, as described for **A** above, has been ruled out by Dance who has argued[6] that protonation of a $-\mu_6$-N nitride in the center of the Fe_6 cavity will have an "impossibly large energy barrier". Further, he argues that while a single N^{3-} ion can pass through an expanded Fe_4 face of the FeMo-cofactor, a protonated N^{3-} cannot. This would be correct if the Fe_6 unit was rigid, but we have determined that this is not the case. The correctly, recognized[6] electronic "plasticity" of the FeMo-cofactor and the severe structural distortions, expected for the Fe_6 prism following reduction and hydration, allow for protonation and removal of the central N^{3-} atom as NH_3 as shown in **C** (Figure 4C).

A very interesting result in the structure of **C** is the location of the two $-\mu_2$-S-bound protons in **B** to positions inside the Fe_6 cage in the corners of the voided-cubane subunits at an H−H distance of 1.86 Å. The structure of **C** (Figure 4C) and the location of the two H atoms are reminiscent of the structure of the P clusters[1−4] where two, closely spaced, Fe_4S_3 units are bridged by a μ_6-S^{2-} ligand (in the space now occupied by the two H atoms in **C**) and two deprotonated cysteinyl residues.[1b,c]

The relocation of the SH protons in **B** to the center of the prismatic cage in **C** has a precedence in a previous DFT study. In this study,[16a] the relocation of a proton from a μ_2-S^{2-} ligand to the interior of the Fe_6 "cage", as an Fe-bound hydride (Fe−H, Å), has been attributed to a large negative electrostatic potential within the central prismatic site. The lowest energy μ_2-S^{2-} site for the H atom was still 42 kJ/mol higher than the Fe_6 hydride site. This lends support to the argument that, in the absence of substantial reorganization energy barriers, relocation of the μ_2-SH^- proton to the center of the cofactor as a hydride could be a facile process.

Removal of the ammonia and water molecules in **C** leads to **D** with a shorter Fe(5)−Fe(6′) distance and the H atoms in approximately the same positions but now showing additional intersubunit Fe−H bonding. In **C** and **D**, the shorter Fe−H distances are found in the range from 1.66 to 1.98 Å (Table 4). It is noteworthy that the total energy of **D** is only 13 kJ/mol higher than that of **H**. This being the case, **D** and **H** could exist in equilibrium that will facilitate the HD exchange (see below and Figure 7).

Dihydrogen complexes[46] show H−H distances of the coordinated H_2 molecule in the range between 1 and 1.1 Å. Distances in excess of 1.5 Å are considered indicative of dihydrides.[47] The long H−H distances in **C** and **D** may therefore indicate that the hydride description is more appropriate. In **D**, the charges on the H atoms, however, are small and positive at 0.00 and +0.10. These values suggest that although reduction of the H^+ must have taken place it still has not reached the hydridic state. Alternatively, if hydrides indeed are present, as suggested by the short Fe−H distances, their negative charges are delocalized over the Fe_6 atoms.

An interesting observation in nitrogenase function is the generation of HD when enzyme turnover is taking place under an atmosphere of D_2.[44,48,49] This exchange suggests that adsorption of H_2 (and D_2) on the cofactor occurs and dissociation of D_2 is followed by HD formation if the two H atoms in **D** approach each other close enough (H−H < 1.5 Å). A possible pathway for HD exchange can be proposed (Figure 7). In this scheme, the ease of H_2 replacement by N_2 (Figure 3, step **D** → **E**) will depend on the extent to which cofactor flexibility (after water addition) allows the two H atoms to approach each other and generate a kinetically labile H_2 molecule.

The apparent affinity of the center of the FeMo-cofactor for the two hydrogen atoms (in **C** and **D**) and also for the N_2 molecule (in **E**) may account for the H_2 inhibition of NH_3 synthesis.[44] Whereas the **D** → **E** conversion as shown in the proposed mechanism (Figure 3) suggests the stoichiometry shown in eq 1, it does not preclude a parallel role for **D** as a H_2-generation catalyst. In such a case, and with a fast rate of H^+ reduction relative to the **D** → **E** conversion, the ratio of H_2 to NH_3 may be greater than 0.5.

Water addition and release of H_2 makes possible the incorporation of N_2 in **E** after the addition of one electron and one proton to **D**. The interactions of the N_2 molecule in **E** with

(43) Shen, B.; Martin, L. L.; Butt, J. N.; Armstrong, F. A.; Stout, C. D.; Jensen, G. M.; Stephens, P. L.; LaMar, G. N.; Gorst, C. M.; Burgess, B. K. *J. Biol. Chem.* **1993**, *268*, 25928.
(44) Burgess, B. K.; Lowe, D. J. *Chem. Rev.* **1996**, *96*, 2983−3011.
(45) H = hartree; 1 H = 2626 kJ = 627.5 kcal.
(46) Kubas, G. J. *Metal Dihydrogen and σ bond complexes: Structure Theory and Reactivity*; Kluwer: New York, 2001 and references therein.
(47) Law, J. K.; Mellows, H.; Heinekey, D. M. *J. Am. Chem. Soc* **2002**, *124*, 1024−1030.
(48) Burgess, B. K. In *Molybdenum Enzymes*; Spiro, T. G., Ed.; Wiley-Interscience: New York, 1985; Chapter 5, pp 161−219.
(49) Thorneley, R. N. F.; Lowe, D. J. In *Molybdenum Enzymes*; Spiro, T. G., Ed.; Wiley-Interscience: New York, 1985; Chapter 5, pp 221−285.

the Fe atoms of the Fe_6 "cage" are unique. The N_2 molecule is oriented along one of the two-fold axes, perpendicular to the three-fold axis of the Fe_6 prism. One of the nitrogen atoms (N1) is nearly equidistant from the four irons that define one of the square faces of the Fe_6 prism with an average Fe−N distance of 2.00 Å. The other N atom (N2) is bound to Fe(5) and Fe(6′) at even shorter distances of 1.89 and 1.87 Å, respectively (Figure 5).

The N−N bond in **E** at 1.33 Å is much longer than the Mo coordinated N_2 in the $(HIPTN_3)MoN_2$ complex (1.061(7) Å). An elongation of the N−N bond to 1.150(5) and 1.156(8) Å is observed in the Mg^{2+} salts of the $1e^-$-reduced derivative $[(HIPTN_3)MoN_2]^-$.[15] The calculated longer N−N distance in **E** indicates N_2 reduction. This is also supported by the calculated charges on N1 (−0.49) and N2 (−0.17), which indicate that the N_2 molecule has undergone reduction, perhaps by as many as two electrons, to N_2^{2-}.

The average charges per Fe atom in the Fe_6 units of **C** and **D** are +0.11 and +0.08, respectively. They are significantly smaller than those in all other intermediates in the $[\mathbf{I\text{-}N\text{-}H}]^{2-}$-based, N_2 reduction cycle (Figure 3), which vary from +0.19 to +0.23. The small positive charges of the Fe atoms in **C** and **D** indicate a metal localized reduction upon addition of three electrons and three protons to **B**. The release of H_2 from **D** and subsequent introduction of N_2 in **E** results in an overall oxidation of the Fe atoms as the N_2 is reduced. It appears that the release of H_2, formally, is more likely due to a combination of available H atoms rather than oxidation of hydrides to H atoms. If this was the case, the Fe_6 atoms should have been reduced.

Binding of N_2 in the center of the FeMo-cofactor, along the Mo to Fe(2′) axis (Figure 1), was originally suggested as a possible N_2-cofactor interaction by Chan et al.[1c] In the same report, however, reservations were expressed for this type of interaction considering the small size of the Fe_6 cavity and its possible inability to accommodate N_2. A similar type of N_2 insertion into the Fe_6 cavity was subsequently proposed by Stavrev and Zerner[18a] on the basis of ZINDO theoretical calculations.

The sequential $2e^-/2H^+$ steps in the **E** → **F** and **F** → **G** conversions (Figure 3) involve the activated N_2 which is converted to an end-bound isodiazene and isohydrazide, respectively. The Fe−N(1) bonds in **F** and **G** are nearly the same and average at 2.03 and 2.02 Å. In **F**, the Fe(5)−N2 bond is 2.04 Å. The N−N bond of the isodiazene in **F** is 1.44 Å and of the isohydrazide in **G** is 1.43 Å. These values and the partial charges on N1 and N2 (Table 3), −0.56, −0.01 and −0.59, +0.19 for **F** and **G**, respectively, clearly show that the greatest extent of N_2 activation has already occurred in the **D** → **E** step. The release of NH_3 from **G** and loss of a water molecule bound to Fe(5) re-forms the Fe(5)−Fe(6′) bond and leads to **A**.

Energetics. The ΔE's associated with the individual steps of the proposed mechanism (Figure 3; Table 6) are shown for both the ESEEM/ENDOR and the Mössbauer models **A**−**G** and $\mathbf{A^0}$−$\mathbf{G^0}$, respectively. They are similar, small, and either positive or negative. The energy of H_2 multiples was taken as a rough estimate of the energy of the added protons and electrons provided by the cellular environment. The largest positive ΔE values of +121 kJ/mol (**F** → **G**) or +92 kJ/mol ($\mathbf{F_0}$ → $\mathbf{G_0}$) are still within the 125 kJ supplied by hydrolysis of 4ATP molecules, presumably consumed in a two electron reduction step.[44] The large negative ΔE of −336 kJ/mol in step **G** → **A** (−320 for $\mathbf{G_0}$ → $\mathbf{A_0}$) shows **A** and $\mathbf{A_0}$ in deep energy minima and may well be the reason the cofactor is isolated in the **A** or $\mathbf{A_0}$ form.

The feasibility of the mechanism proposed here will depend on the activation energies needed to traverse each of the individual steps.

The N_2H_n intermediates proposed, and at times structurally characterized, for the stoichiometric[14] and catalytic[15] reduction of N_2 by mononuclear Mo complexes (Figure 8) are similar to those shown in Figure 3 for $n = 0$, 2, 3, and 4. In the mechanism proposed herein (Figure 3), the N_2H_n intermediates interact with four Fe atoms rather than a Mo atom.

The Role of the Mo Site. The special role that the Mo atom may play in nitrogen fixation has attracted considerable attention, and various theoretical and experimental studies have been reported on Mo-based models. Early coordination chemistry studies on Mo and W, and tertiary phosphine−N_2 complexes, $(P)_4Mo$, by Chatt and co-workers,[14] identified possible key intermediates in the stepwise reduction of dinitrogen. These intermediates include Mo-coordinated nitride, isodiazene, and isohydrazide complexes similar to those reported in this paper (**A**, **F**, and **G**, Figure 3). Such intermediates were also reported (see above) in a very recent study of the catalytic reduction of N_2 by the $(HIPTN_3)MoN_2$ complex (Figure 8). In both of the above studies, a common feature is an end-on Mo-bound N_2 molecule. In the mechanism presented herein (Figure 3), the $(P)_4Mo$[14] or $(HIPTN_3)Mo$[15] activating sites are now replaced by four Fe atoms ($Fe_{3,4,7',8'}$) in the Fe_6 cage.

A scheme for H_2 evolution at the Mo site of the FeMoco and a suggestion that N_2 is subsequently reduced at the same site, following the release of H_2, have been presented.[23,24] In this scheme, protonation of the Mo-coordinated homocitrate ligand generates a coordination site for both hydrogen and dinitrogen reduction.

Earlier we reported on the use of $MoFe_3S_4$ cubanes as catalysts for the reduction of Mo-activated hydrazine[50] and *cis*-dimethyl diazene[51] to ammonia and methylamine, respectively. This work led us to the conclusion that protonated, Mo-bound carboxylate ligands may serve as proton "shuttles".

Theoretical studies on the possible catalytic function of Mo-containing "subsections" of the FeMo-cofactor have been reported.[23] These studies invoke Mo as the site where N_2 binds and subsequently, assisted by a neighboring Fe atom, undergoes reduction to ammonia. Calculations with the N_2 Mo-bound to the FeMo-cofactor, as proposed[22] for the Mo-containing "subsections", and a comparison to **E** show the latter to have a lower energy by ∼26 kJ/mol. The minimum energy structure of the N_2−Mo model, however, shows unrealistically short Fe−Fe distances that range from 2.38 to 2.57 Å. On the basis of comparative protonation studies on model clusters, it has been suggested[52] that the presence of Mo in the FeMo-cofactor may facilitate nitrogen fixation by slowing protonation of the active site and maximizing the opportunity for binding dinitrogen.

(50) (a) Coucouvanis, D.; Mosier, P. E.; Demadis, K. D.; Patton, S.; Malinak, S. M.; Kim, C. G.; Tyson, M. A. *J. Am. Chem. Soc*. **1993**, *115*, 12193. (b) Demadis, K. D.; Coucouvanis, D. *Inorg. Chem*. **1995**, *34*, 3658. (c) Demadis, K. D.; Malinak, S. M.; Coucouvanis, D. *Inorg. Chem*. **1996**, *35*, 4038.
(51) Malinak, S. M.; Simeonov, A. M.; Mosier, P. E.; McKenna, C. E.; Coucouvanis, D. *J. Am. Chem. Soc*. **1997**, *119*, 1662.
(52) Bell, J,; Dunford, A. J.; Hollis, E.; Henderson, R. A. *Angew. Chem., Int. Ed.* **2003**, *42*, 1149.

Most of the proposed mechanisms for the activation and reduction of N_2 centered on the Mo atom are possible or likely, and the chemistry is elegant and sound. The direct relevance of these mechanisms to N_2 fixation by nitrogenase, however, must be evaluated with reference to the entire structure of the FeMo-cofactor.

As indicated in this work, a remarkable six-point attachment and reduction of the N_2 molecule inside the cofactor (Figures 3 and 5E) represents a unique way to activate the N_2 molecule.

In support of the involvement of the Fe_6 center in N_2 activation and reduction (rather than the direct involvement of Mo) is the fact that the Fe_6 unit appears to be a common structural feature in the alternate nitrogenases that contain cofactors with V[53] or Fe[54] in place of Mo. The question still remains: what is the role of the Mo atom (or heteroatom) in the cofactor?

The possibility that structural changes in the FeMoS cluster, brought about by a change in the coordination geometry of the Mo atom, may be of importance in the catalytic function of nitrogenase should be considered.

The effects of the Mo coordination number and geometry on the structure of the $MoFe_3S_3$ cuboidal model clusters are pronounced. Conversion of the six-coordinate Mo atom in $(Cl_4\text{-cat})(L)MoFe_3S_3(CO)_6(PR_3)_2$[11,12] to a five-coordinate, square pyramidal, Mo atom in $(Cl_4\text{-cat})MoFe_3S_3(CO)_6(PR_3)_2$[55] changes a μ_3-S ligand in the former to a quasi-terminal sulfido ligand in the latter (Mo═S, 2.213(1) Å). This nascent sulfido ligand shows only weak bonding to two of the core Fe atoms. As a result, the $MoFe_3S_3$ cuboidal unit is now severely distorted.

The structure of the FeMoS center in nitrogenase shows the Mo atom anchored to the protein by a histidine imidazole (Mo−Nδ1 interaction). Recent calculations show[16a] that, upon protonation, the Mo−Nδ1 bond cleaves and the nitrogen donor moves away from the molybdenum by nearly 3.5 Å. The end result of such an event is a change in the structure of the cofactor which now contains a five-coordinate molybdenum atom coordinated by three μ_3-sulfido groups. The latter, by analogy to the model clusters previously discussed, may rearrange to square pyramidal geometry as one of the cluster sulfido ligands (a nascent Mo−S_{ax} group) is converted to an axial thiomolybdenyl group. Subsequent structural changes within the FeMoS core are expected to follow.

We suggest that changes in the coordination geometry of the heteroatom in the cofactor of nitrogenase (Mo, V), brought about by pH changes, may result in subtle changes in the cofactor structure. Such changes may further facilitate N_2 binding.

Summary and Conclusions

This study underscores a number of structural and electronic characteristics of the FeMo-cofactor of nitrogenase. Some of these characteristics were pointed out in earlier theoretical studies; others are newly recognized and may be important for the activation and catalytic reduction of N_2.

There is little doubt that a light atom occupies the center of the Fe_6 cavity. As originally suggested, this atom is generally accepted as N^{3-}. Our calculations support the presence of a light atom and show the center-voided FeMo-cofactor with considerably higher energy. Our results, however, are not as "clear-cut" as previous results, and our assignment of the central atom as N^{3-} (vs O^{2-}) is preferred with marginal certainty.

Earlier DFT calculations showed the migration of an μ_2-S-bound H^+ to the center of the FeMo-cofactor as a hydride. The center of the Fe_6 cavity was considered as a site of a "large negative electrostatic potential". This observation is substantiated in our studies. The introduction of N_2 in the center of the FeMo-cofactor occurs with partial reduction of N_2 and elongation of the N−N bond. Indeed the six-Fe activation of N_2 is remarkable and only possible with the unique cofactor structure.

The distortion of the Fe_6 site, needed for the insertion of the N_2 molecule and any subsequent addition of protons, occurs readily. It is energetically feasible when one of the μ_2-S ligands is protonated and the Fe−Fe intersubunit "bond" is solvolyzed. These events lead to an elongation of the Fe−Fe distance which is facilitated by the coordination of SH and H_2O as terminal ligands to the originally μ_2-S-bridged Fe atoms (see conversions **A** → **B** and **D** → **E**, Figure 3). Very recently, a DFT calculation[56] examining nitrogen binding to the FeMo-cofactor has been reported. In this study, binding of N_2 to an Fe site next to a protonated μ_2-S bridge leads to rupture of the μ_2-S bridge and elongation of the Fe−Fe distance.

The electron density within the FeMo-cofactor is highly delocalized, and oxidations or reductions are "smeared-out " throughout the cluster. The experimentally derived different oxidation states for the Fe atoms, obtained by analyses of either Mössbauer or ENDOR/ESEEM spectra, are not clearly discernible. Similarly, protonation of the three μ_2-S ligands in the cofactor, although it results in significantly longer μ_2-S distances, does not lead to appreciable differences in the atomic charges obtained by MPA.

The in-cavity, end-on, N_2 interaction with the FeMo-cofactor (**E**, Figure 3, Figure 5E) shows all six Fe atoms interacting with N_2. The interactions of N(1) with $Fe_{3,4,7',8'}$ are similar to proposed interactions of an end-on-bound N_2 to the 100 face of the metallic iron catalyst in the Haber−Bosch ammonia synthesis.[57] This type of interaction and structures for the isodiazene and isohydrazide intermediates (**F**, **G**, Figures 3, 5F,G) are similar to those proposed or determined for the $(P)_4Mo$[13] or $(HIPTN_3)Mo$[14] complexes encountered in either stoichiometric[14] or catalytic[15] reductions of N_2.

The role of the Mo atom (or the V and Fe heteroatoms in the alternate nitrogenases) is not clear. At this stage, one can only speculate that changes in the coordination geometry of the heteroatom, brought about by pH changes and ligand protonation, may bring changes to the FeMo-cofactor structure that assist in mechanistic pathways. Structural studies of the Roussin-type clusters with the $MoFe_3S_3$ cores[55] show pronounced cluster structural changes upon changes in the coordination number of the Mo atoms.

Acknowledgment. D.C. acknowledges the continued support of this research by the NIH (GM33080). In the University of

(53) (a) Davis, R.; Lehman, L.; Petrovich, R.; Shah, V. K.; Roberts, G. P.; Ludden, P. W. *J. Bacteriol.* **1996**, *178*, 1445 and references therein. (b) Gollan, U.; Schneider, K.; Muller, A.; Schudderkopf, K.; Klipp, W. *Eur. J. Biochem.* **1993**, *215*, 25.
(54) Krahn, E.; Weiss, B. J. R.; Kroeckel, M.; Groppe, J,; Henkel, G.; Cramer, S. P.; Trautwein, A. X.; Schneider, K.; Mueller, A. *J. Biol. Inorg. Chem.* **2002**, *7*, 37.
(55) Tyson, M. A.; Coucouvanis, D. *Inorg. Chem.* **1997**, *36*, 3808.
(56) Schimpl, J.; Petrill, H. M.; Blochl, P. E. *J. Am. Chem. Soc.* **2003**, *125*, 15772.
(57) Bozso, F.; Ertl, G.; Grunze, M.; Weiss, M. *J. Catal.* **1977**, *49*, 18.

Karlsruhe, this work is supported by the Center for Functional Nanostructures (CFN) of the Deutsche Forschungsgemeinschaft (DFG) within project C2.2. D.C. is indebted to the chemistry faculty at the University of Karlsruhe for their exquisite hospitality during his latest sabbatical leave there.

Supporting Information Available: Tables giving Cartesian coordinates for DFT energy optimized structures, and Mulliken population analyses and net spins for all atoms, for the dianions **A**, **B**, **C**, **D**, **E**, **F**, **G**, and **H**. Mechanistic intermediates calculated using the EPR/ENDOR model. Tables giving Cartesian coordinates MPA charges and net spins for energy optimized structures for $\mathbf{A^0}$, $\mathbf{B^0}$, $\mathbf{C^0}$, $\mathbf{D^0}$, $\mathbf{E^0}$, $\mathbf{F^0}$, $\mathbf{G^0}$, and $\mathbf{H^0}$. Mechanistic intermediates calculated using the Mössbauer model. Similar tables for calculations using a methanethiolate ligand in place of the chloro ligand on the Fe(2′) atom. Figures for **A**, **B**, **C**, **D**, **E**, **F**, and **G** (PDF). This material is available free of charge via the Internet at http://pubs.acs.org.

JA030541Z